

Detection of particle-phase polycyclic aromatic hydrocarbons in Mexico City using an aerosol mass spectrometer

Katja Dzepina^{a,b}, Janet Arey^c, Linsey C. Marr^{d,1}, Douglas R. Worsnop^e, Dara Salcedo^f,
Qi Zhang^{a,2}, Timothy B. Onasch^e, Luisa T. Molina^{d,3}, Mario J. Molina^{d,g}, Jose L. Jimenez^{a,b,*}

^a Cooperative Institute for Research in the Environmental Sciences (CIRES), University of Colorado at Boulder, Boulder, CO, United States

^b Department of Chemistry and Biochemistry, University of Colorado at Boulder, Boulder, CO, United States

^c University of California at Riverside, Air Pollution Research Center, Riverside, CA, United States

^d Department of Earth, Atmospheric and Planetary Sciences, Massachusetts Institute of Technology, Cambridge, MA, United States

^e Center for Aerosol and Cloud Chemistry, Aerodyne Research, Inc., Billerica, MA, United States

^f Centro de Investigaciones Químicas, Universidad Autónoma del Estado de Morelos, Cuernavaca, Morelos, Mexico

^g Department of Chemistry and Biochemistry, University of California at San Diego, La Jolla, CA, United States

Received 14 May 2006; received in revised form 28 December 2006; accepted 18 January 2007

Available online 25 January 2007

Abstract

We report the quantification of ambient particle-bound polycyclic aromatic hydrocarbons (PAHs) for the first time using a real-time aerosol mass spectrometer. These measurements were carried out during the Mexico City Metropolitan Area field study (MCMA-2003) that took place from March 29 to May 4, 2003. This was the first time that two different fast, real-time methods have been used to quantify PAHs alongside traditional filter-based measurements in an extended field campaign. This paper focuses on the technical aspects of PAH detection in ambient air with the Aerodyne AMS equipped with a quadrupole mass analyzer (Q-AMS), on the comparison of PAHs measured by the Q-AMS to those measured with the other two techniques, and on some features of the ambient results.

PAHs are very resistant to fragmentation after ionization. Based on laboratory experiments with eight PAH standards, we show that their molecular ions, which for most particulate PAHs in ambient particles are larger than 200 amu, are often the largest peak in their Q-AMS spectra. Q-AMS spectra of PAH are similar to those in the NIST database, albeit with more fragmentation. We have developed a subtraction method that allows the removal of the contribution from non-PAH organics to the ion signals of the PAHs in ambient data. We report the mass concentrations of all individual groups of PAHs with molecular weights of 202, 216, 226 + 228, 240 + 242, 250 + 252, 264 + 266, 276 + 278, 288 + 290, 300 + 302, 316 and 326 + 328, as well as their sum as the total PAH mass concentration.

The time series of the Photoelectric Aerosol Sensor (PAS) and Q-AMS PAH measurements during MCMA-2003 are well correlated, with the smallest difference between measured PAH concentrations observed in the mornings when ambient aerosols loadings are dominated by fresh traffic emissions. The Q-AMS PAH measurements are also compared to those from GC–MS analysis of filter samples. Several groups of PAHs show agreement within the uncertainties, while the Q-AMS measurements are larger than the GC–MS ones for several others. In the ambient Q-AMS measurements the presence of ions tentatively attributed to cyclopenta[cd]pyrene and dicyclopentapyrenes causes signals at m/z 226 and 250, which are significantly stronger than the signals in GC–MS analysis of filter samples. This suggests that very labile, but likely toxic, PAHs were present in the MCMA atmosphere that decayed rapidly due to reaction during filter sampling, and this may explain at least some of the differences between the Q-AMS and GC–MS measurements.

© 2007 Elsevier B.V. All rights reserved.

Keywords: AMS; PAH; Mexico City

* Corresponding author.

E-mail address: jose.jimenez@colorado.edu (J.L. Jimenez).

¹ Present address: Department of Civil and Environmental Engineering, Virginia Tech, Blacksburg, VA, United States.

² Present address: Atmospheric Sciences Research Center, University at Albany, SUNY, Albany, NY, United States.

³ Present address: Molina Center for Energy and Environment, La Jolla, CA, United States.

1. Introduction

Polycyclic aromatic hydrocarbons (PAHs) are products of incomplete combustion formed during the burning or pyrolysis of organic matter, and are released into ambient air from a wide range of combustion sources, such as diesel and gasoline engines, biomass burning of agricultural and forest fuels, coal combustion, and wood smoke [1,2]. Fossil fuels such as gasoline or diesel fuel also contain PAHs, which may escape the combustion process [1]. Depending on their molecular weight (which is inversely related to their vapor pressure), PAHs in ambient air will be found in the gas-phase (e.g., 2-ring naphthalene), particulate phase (e.g., 5-ring benzo[*a*]pyrene), or will partition between gas- and particle-phases (e.g., 3-ring phenanthrene and 4-ring pyrene) [3].

Due to the carcinogenicity and mutagenicity of certain PAHs, the U.S. EPA has defined 16 “Priority PAH Pollutants” [2,4]. Many PAHs, after metabolic activation, can induce lung and skin tumors in laboratory animals [5]. Very recently, benzo[*a*]pyrene was classified as a Group 1 (“carcinogenic to humans”) carcinogen and cyclopenta[*cd*]pyrene, dibenz[*a,h*]anthracene and dibenzo[*a,l*]pyrene as Group 2 (“probably carcinogenic to humans”) carcinogens [5]. Fine particles, with their adsorbed burden of PAHs, can penetrate deeply into the human lung and be deposited there, and have been associated with short and long term human health effects [6–9]. The toxicity of some PAHs and some of their atmospheric reaction products, coupled with the ability of fine particles to deliver these toxics to the human lung, makes the rapid detection of particle-phase PAHs important.

Mass spectrometry (MS) coupled to gas or liquid chromatography (GC or LC, respectively) has been extensively used in the quantitative detection of particle-phase PAH in samples previously collected on filters. This type of analysis typically requires significant sample preparation and is typically used with time resolutions of several hours to a day. A large literature exists on those types of analyses [e.g., 10]. Two types of PAH analysis methods have been reported that use real-time or near-real time mass spectrometry. Off-line but quantitative and highly time-resolved (20 min) particle-phase PAH measurements have been recently carried out by combining sampling with a rotating drum impactor and analysis by two-step laser mass spectrometry (L2MS) [11,12]. Single-particle laser desorption/ionization (LDI) time-of-flight mass spectrometry has been used for the on-line qualitative detection of PAHs from soot particles [13,14] and vehicle exhaust [15–17]. In this paper, we present the first real-time quantitative ambient measurements of particle-phase PAHs that use an aerosol mass spectrometer.

The Mexico City Metropolitan Area (MCMA-2003) field study took place from March 29 to May 4, 2003. With the participation of many research groups and the use of an array of advanced instrumentation, it represented the most complete study of Mexico City’s atmosphere prior to the MILAGRO 2006 field campaign. During MCMA-2003, particle-bound PAHs were measured by three different methods: (1) collection and GC–MS analysis of filter samples; (2) aerosol photoioniza-

tion, a fast specific method of detecting PAHs on particles’ surfaces with a Photoelectric Aerosol Sensor (PAS); and (3) aerosol mass spectrometry (AMS), a rapid method of analyzing particle size and chemical composition. In this paper, we’ll use “PAH” for the general class of compounds, and “FPAH”, “SPA” and “APAH”, respectively, to distinguish between particle-bound PAHs measured by the three methods. A detailed description and intercomparison of the MCMA-2003 total particle-phase PAH ambient concentrations measured by the three techniques, as well as a study of the PAH transformations in the Mexico City atmosphere, are given in a separate publication [18].

A recent laboratory study [19] has demonstrated the capability of using the Q-AMS to detect PAHs in/on particles generated in a laboratory propane flame. The AMS has been used extensively in laboratory [e.g., 20–22] and both ground-based and aircraft-based field studies [e.g., 23–27] to measure the concentration of inorganic and organic aerosol species. However the quantification and detection of PAHs in ambient air using an AMS has not been reported to our knowledge.

In this paper, we report the technical approach for PAH detection in ambient air with the Aerodyne Q-AMS, including the subtraction method developed to remove non-PAH organic interferences and its assumptions and limitations. The Q-AMS ambient spectra are compared with those measured when sampling pure PAH standards and laboratory flame-generated particles, as well as with NIST database spectra. We present emission ratios of PAHs to other primary pollutants, comparison of PAS and Q-AMS PAH time series, and detailed comparisons between PAH concentrations from GC–MS analysis of filter (and filter/adsorbent) samples and the Q-AMS PAH measurements. Finally, we report the size distributions of PAHs with molecular weights of 202 and 226.

2. Experimental

The AMS allows real-time, size and composition analysis of non-refractory submicron atmospheric aerosol particles (NR-PM₁). Several versions of the Aerodyne AMS are available at present: Q-AMS with a quadrupole mass spectrometer, C-ToF-AMS with a time-of-flight mass spectrometer [28] and a HR-ToF-AMS with a high resolution ToF mass spectrometer [29]. In this paper, we will use “Q-AMS” for the quadrupole based instrument (as used during MCMA-2003) and “AMS” when the statements are true for all AMS types. A detailed description of the Q-AMS like the one used during MCMA-2003 can be found elsewhere [23,30]. Briefly, particles are sampled from ambient pressure, and are focused using an aerodynamic lens into a narrow beam and introduced into a particle sizing vacuum chamber [31–34]. Particle vacuum aerodynamic diameter [22,35] is determined by measuring the time it takes a particle to reach the detector after passing a particle chopper shortly after the end of the lens. Next, particles impact on a heated surface at ~600 °C, leading to flash vaporization followed by electron impact (EI) ionization of the vapor molecules, which produces positive ions. Finally, particle chemical composition is obtained by the analysis of the ions by a quadrupole mass spectrometer

(Balzers QMA 410). Mass discrimination for this quadrupole mass spectrometer is negligible below m/z 330 according to the manufacturer.

During the MCMA-2003 campaign a Q-AMS was located at the highly instrumented “Supersite” housed in the building of National Center for Environmental Research and Education (“Centro Nacional de Investigación y Capacitación Ambiental” or CENICA). CENICA is located at the Universidad Autónoma Metropolitana campus Iztapalapa (UAM-I) in the south east of Mexico City. Q-AMS data were recorded every four minutes. The detailed description of Q-AMS operation, calibrations and overview of the results during MCMA-2003 are presented by Salcedo et al. [36]. The time series of all APAH data presented in this paper have a 4-point boxcar smoothing applied to reduce high-frequency noise in the data. All the data presented in this paper are shown in local time and at local temperature and pressure conditions.

During MCMA-2003, PAHs were also measured with two other methods: PAS and GC–MS analysis of filter samples. These methods and their application to this study have been described in detail elsewhere [18]. Briefly, in aerosol photoionization the aerosol sample is exposed to ultraviolet light from an excimer lamp at 207 nm, causing PAHs on the surface of particles to photoemit electrons. The ejected electrons are removed by an electric field, and the positively charged particles are trapped on a filter, generating a current that is measured by an electrometer. A high-volume air sampler equipped with a Teflon-impregnated glass fiber filter and two polyurethane foam plugs (PUFs) in series beneath the filter and without a denuder or size-selective inlet was used to collect particle-associated and semi-volatile gas-phase PAHs, respectively. These filters and PUFs were analyzed by GC–MS for PAHs of MWs 202, 216, 226, 228, 240, 242, 252, 276 and 300 for 2 days overlapping with the Q-AMS measurements, on April 27 and on April 29, 2003. Filter samples were collected during four consecutive time periods: morning samples from 7 a.m. to 11 a.m., day samples from 11 a.m. to 4 p.m., evening samples from 4 p.m. to 9 p.m., and night samples from 9 p.m. to 7 a.m.

Laboratory Q-AMS experiments were also performed for the following eight PAH standards: pyrene (98%, Aldrich), 2,3-benzofluorene (98%, Aldrich), 1-methylpyrene (>97%, Fluka), triphenylene (98%, Aldrich), 10-methylbenz[*a*]anthracene (Sigma–Aldrich), benzo[*e*]pyrene (99%, Aldrich), benzo[*ghi*]perylene (98%, Aldrich) and coronene (99%, Aldrich). Each of the eight PAH standards was dissolved in 2-propanol (Iso-propanol UN1219 suitable for electronic use, Fisher Scientific), atomized (TSI 3076 Constant Output Atomizer), dried with three silica gel diffusion driers in series and introduced into the Q-AMS. The vaporizer was maintained at the standard AMS temperature of $\sim 600^\circ\text{C}$ when sampling these PAH standards. With the same Q-AMS instrument, we measured the relative ionization efficiencies (RIEs) of the 1-methylpyrene, triphenylene and 10-methylbenz[*a*]anthracene PAH standards. The same instrumental set-up as above was used, with the addition of an Electrostatic Classifier (TSI 3080) for the selection of 350 nm mobility diameter particles, and a Condensation Particle Counter (TSI 3022A).

3. Results and discussion

3.1. Determination of PAH concentrations from Q-AMS data

3.1.1. Laboratory PAH standards and flame Q-AMS spectra

Aromatic rings such as those in PAHs are very resistant to fragmentation after ionization due to the stabilizing effects of their delocalized π -electrons [37]. Thus, the molecular ion is normally observed with significant intensity, even with a relatively hard ionization technique such as electron impact (EI). The EI mass spectra of PAHs generally consist of intense molecular ion peaks, smaller ions due to the loss of one to four hydrogen atoms, and doubly charged ions with about 20% of the abundance of the molecular ion [38]. The molecular ions of most PAHs present in the particle phase in ambient air are larger than 200 amu [2]. In a Q-AMS, if the species are vaporized intact, their mass spectra are generally similar to the standard EI spectra such as in the NIST database [39]. However, due to the higher internal energy acquired during vaporization in the AMS or to decomposition of thermally labile species during the vaporization process, the spectra observed in the AMS for various organic species may show greater fragmentation than standard EI spectra [40]. In order to examine the fragmentation behavior of PAH in the Q-AMS mass spectra, we carried out laboratory experiments with pure particles of eight PAH standards. Fig. 1 compares the laboratory Q-AMS and NIST database mass spectra of pyrene, 1-methylpyrene and 2,3-benzofluorene. Similar comparisons for the other five PAHs mass spectra are presented in the [Supplementary Information \(Figures SI-1 and SI-2\)](#). The Q-AMS spectrum of pyrene is very similar to the NIST database spectrum. Both Q-AMS and NIST database spectra show the same most intense m/z (“base peak”) and group of peaks, but the Q-AMS spectra shows greater fragmentation. The increase in fragmentation with the Q-AMS versus NIST mass spectra was observed for all PAH, and is analyzed quantitatively in Section 3.1.5. Enhanced PAH fragmentation has also been observed in Laser Microprobe Mass Spectrometry (LMMS) where a laser pulse causes sample ablation and ionization [41].

PAHs with an odd number of carbons (“o-PAHs”) cannot be completely conjugated and are generally less stable [42] and less abundant in soot [43] (see [Table 1](#) for examples). o-PAHs can be either methyl-substituted fully benzenoid PAHs (e.g., 1-methylpyrene) or contain a $-\text{CH}_2-$ group, generally in a 5-membered ring (e.g., benzofluorenes). In standard EI mass spectra, methyl-PAHs show more intense $[M - 1]$ fragments than the fully benzenoid PAHs do, and methylene structures (such as fluorene) show $[M - 1]/M$ ratios around unity [44]. The Q-AMS spectra of 1-methylpyrene and 2,3-benzofluorene in Fig. 1b and c are similar to the NIST database spectra with the same groups of peaks present and significantly larger fragmentation. However there is another important difference: the base peaks are not the molecular ions, but the molecular ions minus one. The increased importance of the $[M - 1]$ peak resulting from H loss of the molecular ion, that often becomes the base peak, is observed for all o-PAHs analyzed by the Q-AMS. This effect was also observed in analysis of particle-bound PAHs pro-

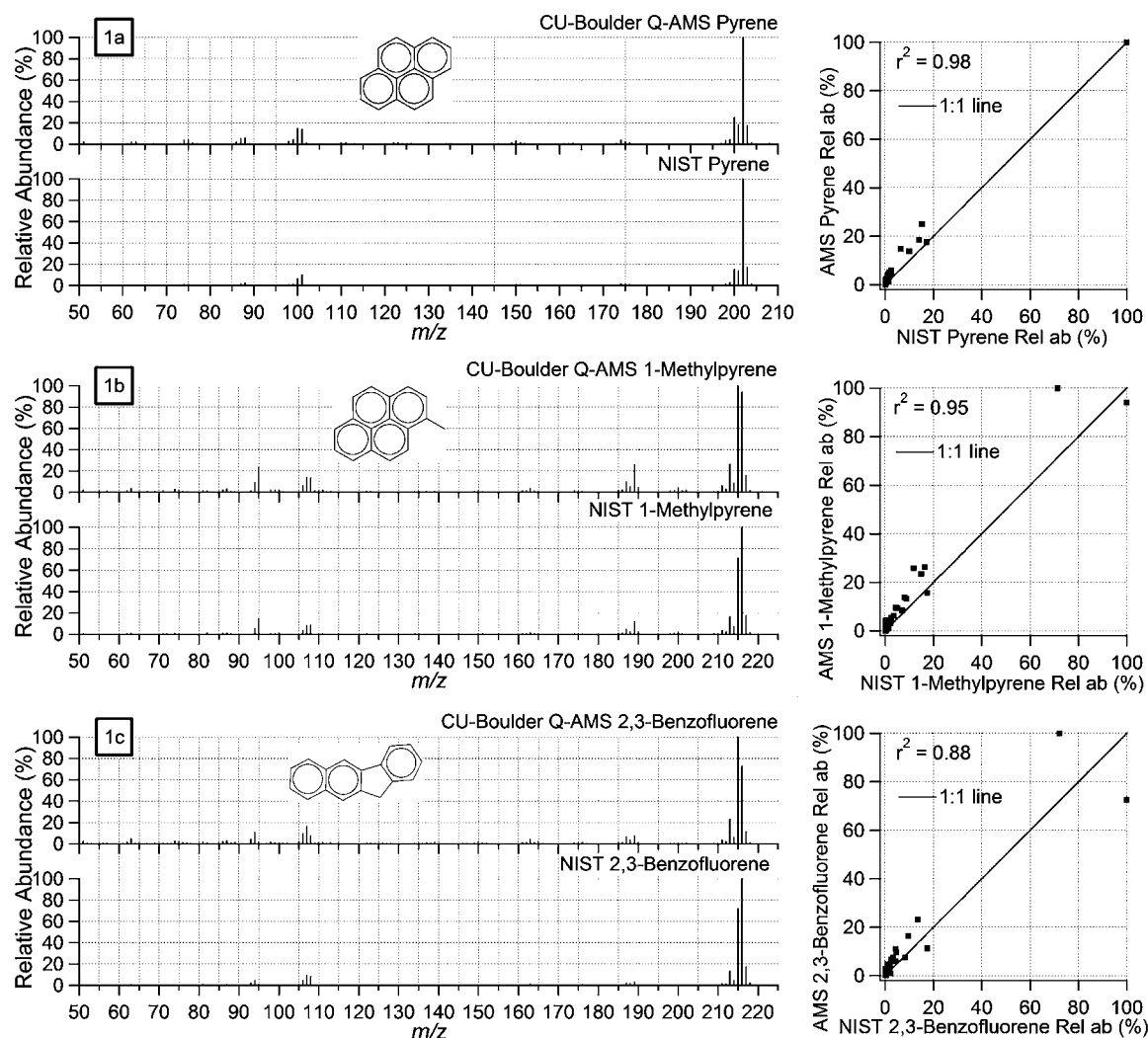


Fig. 1. Left: pyrene, 1-methylpyrene and 2,3-benzofluorene laboratory mass spectra for NIST database and for pure standards sampled with the Q-AMS. Right: scatter plots between the AMS and NIST database mass spectra of PAH standards.

duced in a laboratory propane flame [19]. These o-PAHs also seem to be fragmenting in the same manner in our ambient measurements. Some of these o-PAHs (such as benzo[c]fluorene at MW = 216) have been shown to be toxic and carcinogenic [45]; thus, it is important to include them in the total PAH mass concentrations measured.

3.1.2. Non-PAH organic interference subtraction procedure

Zhang et al. [46] have recently shown that the AMS organic spectrum at high m/z ratios in an urban area was dominated by primary combustion emissions. EI ionization is not specific to PAHs, and fragments of other organic species can also be present at the same m/z values as the PAH ions. For example, long-chain alkanes, branched alkanes, or alkyl aromatics are known to comprise a significant fraction of the organic aerosol mass in vehicle exhaust [47–49]. These species can produce many different fragments above m/z 200. Thus, ions from PAHs and various non-PAH organics in a Q-AMS mass spectrum can overlap at the same integer m/z ratios. The Q-AMS used during MCMA-2003 has unit m/z resolution, and thus is not able

to directly separate the PAH and aliphatic signals at the same m/z . For this reason we have developed a subtraction method to estimate the contributions of PAH and non-PAH organics to the signal at a given m/z .

This method is based on the observation that ambient non-PAH organics in urban areas produce a relatively predictable AMS spectral pattern above m/z 200 where peak intensity decays monotonically as m/z increases with most peaks not sticking out significantly above their neighbors [46]. Odd m/z peaks typically have higher signal levels than even m/z peaks due to the fragmentation properties of hydrocarbons [37], but the envelope of both series stays approximately parallel to each other as the signal decreases towards high m/z . Ion signals from PAH are “added” on top of this regularly decreasing pattern. This allows the approximate subtraction of the contribution from non-PAH organics to the ion signals of the PAHs according to the following assumptions and approach:

- The non-PAH organic signal in the vicinity of a particular PAH molecular ion decreases monotonically with m/z and

Table 1

Examples of structures, common names, empirical formulas and molecular weights of PAHs that partition into the particle phase

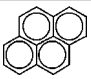
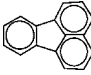
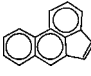
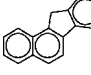
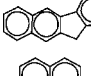
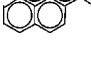
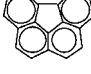
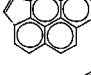
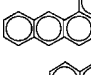
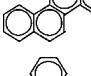
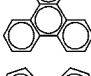
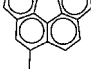
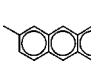

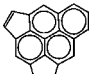
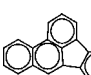
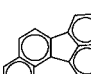
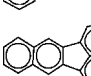
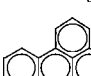
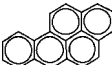
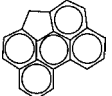
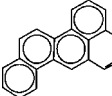
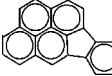
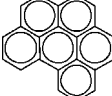
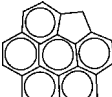
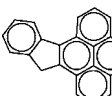
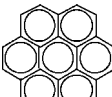
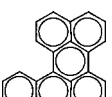
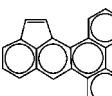
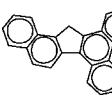
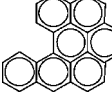
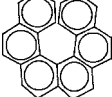
Structure	Common name	Empirical formula	Molecular weight (g mol ⁻¹)	April 29, 2003 7–11 a.m. average FPAH mass conc. (ng m ⁻³) Filter (PUF)
	Pyrene	C ₁₆ H ₁₀	202	1.9 (10.3)
	Fluoranthene	C ₁₆ H ₁₀	202	1.4 (7.8)
	Acephenanthrylene	C ₁₆ H ₁₀	202	0.3 (1.4)
	1,2-Benzofluorene (11H-benzo[a]fluorene)	C ₁₇ H ₁₂	216	0.3
	2,3-Benzofluorene (11H-benzo[b]fluorene)	C ₁₇ H ₁₂	216	0.2
	1-Methylpyrene	C ₁₇ H ₁₂	216	0.1 4 additional FPAH peaks: 0.5 (Total 216 on PUF: 3.3)
	Benzo[ghi]fluoranthene	C ₁₈ H ₁₀	226	2.0
	Cyclopenta[cd]pyrene	C ₁₈ H ₁₀	226	2.2
	Benz[a]anthracene	C ₁₈ H ₁₂	228	1.6
	Chrysene	C ₁₈ H ₁₂	228	Chrysene + Triphenylene: 2.6
	Triphenylene	C ₁₈ H ₁₂	228	
	Methylbenzo[ghi]fluoranthene	C ₁₉ H ₁₂	240	Up to 3 FPAH peaks: 0.6
	10-Methylbenz[a]anthracene	C ₁₉ H ₁₄	242	Up to 10 FPAH peaks: 1.8
	Corannulene	C ₂₀ H ₁₀	250	See discussion in Section 3
	Dicyclopenta[cd,mn]pyrene	C ₂₀ H ₁₀	250	
	Benzo[b]fluoranthene	C ₂₀ H ₁₂	252	Benzo[b]fluoranthene + Benzo[j]fluoranthene + Benzo[k]fluoranthene: 6.3
	Benzo[j]fluoranthene	C ₂₀ H ₁₂	252	
	Benzo[k]fluoranthene	C ₂₀ H ₁₂	252	
	Benzo[e]pyrene	C ₂₀ H ₁₂	252	3.2

Table 1 (Continued)

Structure	Common name	Empirical formula	Molecular weight (g mol ⁻¹)	April 29, 2003 7–11 a.m. average FPAH mass conc. (ng m ⁻³) Filter (PUF)
	Benzo[a]pyrene	C ₂₀ H ₁₂	252	3.4
	11H-Cyclopenta[ghi]perylene (*)	C ₂₁ H ₁₂	264	
	4H-Benzo[hi]chrysene (*)	C ₂₁ H ₁₄	266	
	Indeno[1,2,3-cd]pyrene	C ₂₂ H ₁₂	276	5.3
	Benzo[ghi]perylene	C ₂₂ H ₁₂	276	12.9
	1H-Benzo[ghi]cyclopenta[pqr]perylene (*)	C ₂₃ H ₁₂	288	
	9H-Indeno[1,2-e]pyrene (*)	C ₂₃ H ₁₄	290	
	Coronene	C ₂₄ H ₁₂	300	4.7
	Benzo[a]perylene (*)	C ₂₄ H ₁₄	302	
	Indeno[1,7-ab]triphenylene (*)	C ₂₄ H ₁₄	302	
	15H-Benz[4,5]indeno[1,2-l]-phenanthrene (*)	C ₂₅ H ₁₆	316	
	Dibenzo[a,ghi]perylene (*)	C ₂₆ H ₁₄	326	
	Phenanthro[3,4-c]phenanthrene (*)	C ₂₆ H ₁₆	328	

Except with those marked with an asterisk (*), all have been detected in GC–MS mass spectra of filter-collected PAHs during MCMA-2003 (FPAH). As an example, the mass concentrations of several FPAH quantified by GC–MS in a April 29, 2003 morning sample are given.

has an approximately linear trend, in two separate series for even and odd m/z values.

- (b) The non-PAH signal at the PAH molecular ion (MI) peak, as well as at four m/z values below the MI (based on

the observed fragmentation pattern in laboratory spectra described above) is estimated by weighted average of the signal at four neighboring peaks (two above and two below this group of peaks) to which PAHs are known not to pro-

duce an ion signal. The estimation of the organic signal at even PAH m/z values includes only even organic peaks, and the estimation of the organic signal at odd PAH m/z values includes only odd organic peaks. The weighted average takes into account the distance between the PAH and non-PAH m/z 's used. The detailed description of the procedure is given in [Appendix 1 \(Supplementary Information\)](#).

- (c) The signals attributed to PAHs at the molecular ion peak and at four m/z values below are estimated as the difference between the total signal at the known m/z of PAH peaks and the estimated non-PAH organic signal at those peaks.
- (d) For each pair in the groups of PAHs with MWs 226 + 228, 240 + 242, 250 + 252, 264 + 266, 276 + 278, 288 + 290, 300 + 302 and 326 + 328, we cannot distinguish the contributions of each group to several of the m/z 's. Thus, we report the mass concentrations of those PAHs as the sum of both MW groups of PAHs in the pair.
- (e) The PAH signal at one m/z above the larger molecular ion of each group of PAHs is estimated as the ^{13}C isotopic contribution from the PAH signal at its molecular ion [37].

These subtraction and fragmentation rules are implemented in the Q-AMS data analysis software using the “fragmentation table” approach of Allan et al. [50]. The detailed formulae are given in [Appendix 2 \(Supplementary Information\)](#). The signals at each group of peaks are summed to produce the total signal for all PAHs of given molecular weights, which for the AMS should be proportional to their mass concentration [23]. Finally, the signals from PAHs of all molecular weights are added together to produce the total PAH signal. Only 4-ring or larger (i.e., MW > 200) PAHs have been added to the total AMS PAH mass concentration in this study.

In a recent AMS study of industrial process effluents it was observed that the non-PAH organics had a strong 14-amu series [F. Drewnick, Max Planck, pers. comm., 2006], which is very different from what we observed during MCMA-2003. The general subtraction approach developed here should still be applicable to such data, although the detailed subtraction rules might need to be adapted to the features of the non-PAH background.

Even though their presence in ambient particles is suspected based on inspection of some source or ambient spectra, PAHs with MW 152, 166 and 190 have not been added to the total AMS

PAH mass concentration in this study. These 2- and 3-aromatic ring PAHs tend to reside in the gas-phase, so that a smaller fraction of their concentrations is in the particle phase. Their PM concentrations can in some cases be comparable to the PAHs of higher molecular weights due to their higher overall concentrations [2]. However their direct estimation from Q-AMS spectra using subtraction rules would be more uncertain, as these peaks are surrounded by a larger and more variable non-PAH organic signal than PAHs above m/z 200. Gas-particle partitioning theory [51] has been shown to accurately predict the gas/particle partitioning of PAHs [e.g., 52]. In order to estimate the contribution of 2- and 3-aromatic ring PAHs to the total particulate PAH mass loadings we have used partitioning theory with the temperature minimum during the whole MCMA-2003 AMS sampling period (11 °C, in order to find the maximum partitioning to the particle phase), the average organic mass measured (20 $\mu\text{g m}^{-3}$) and an assumed activity coefficient of 1. The calculated percent of particle-phase partitioning for 2-ring naphthalene and 3-ring phenanthrene is 0.01% and 4.46%, respectively. Compared to the naphthalene and phenanthrene highest measured gas-phase concentrations [Arey, Reisen and Bethel, unpublished data] for the morning of April 29, 2003 of 5000 ng m^{-3} and 45 ng m^{-3} , respectively, the upper limits for their particulate mass loadings will account for 0.5 ng m^{-3} and 2.0 ng m^{-3} , respectively. By comparison with the PAH levels reported by Marr et al. [18] and later in this paper, we conclude that the partitioning of 2- and 3-aromatic ring PAHs is a very small fraction (a few percent at the most) of the total particulate PAH mass loadings during this study. Thus, the APAH concentrations reported here should be representative of the total particle-phase PAH.

3.1.3. Results of the interference subtraction procedure

Fig. 2 compares mass spectra of PAH-dominated particles generated in a laboratory propane flame study [19] and the average rush hour PAH mass spectra (all MCMA-2003 5 a.m.–9 a.m. periods) obtained using the subtraction rules just described. There is a good correlation ($r^2 = 0.72$) between these two laboratory and ambient mass spectra, which is reduced significantly (to $r^2 = 0.36$) if the subtraction procedure is not applied to the Q-AMS data. The similarity between the two spectra and the increase in r^2 after applying the subtraction procedure support

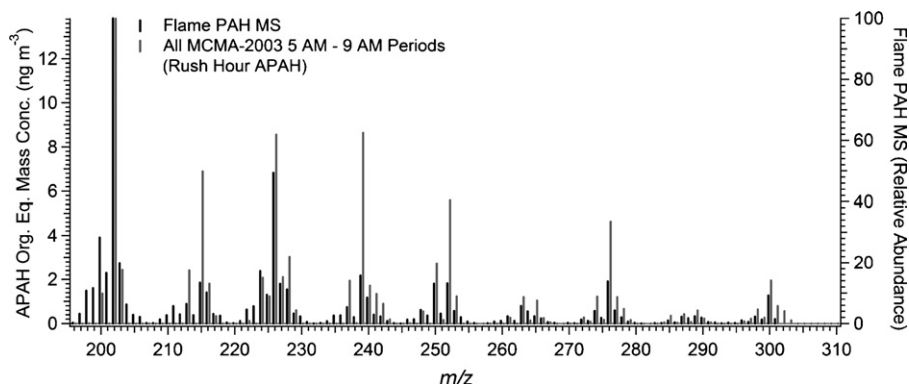


Fig. 2. Comparison of the total (PAH + Organics) Q-AMS mass spectra of PAH-dominated particles generated in a laboratory propane flame study [19] and the average rush hour PAH Q-AMS mass spectra (all MCMA-2003 5 a.m.–9 a.m. periods).

Table 2

Main statistical parameters for the total and modified total (APAH and APAH^{*}, respectively) AMS PAH concentrations and its contributing PAH groups

MW of APAH	Average	Standard deviation	Median	Maximum	Minimum	% of negative APAH	1-h DL ($3 \times \sigma$)
Total APAH	58.5	65.7	42.7	1593.4	−61.3	5.1	15.4
Total APAH [*]	34.5	46.9	24.3	1348.0	−70.7	8.1	8.0
202	11.4	14.1	9.1	279.0	−116.3	10.5	4.4
216	9.4	10.2	7.7	174.5	−49.6	10.0	4.1
226 + 228	10.2	17.5	6.8	419.7	−81.7	17.8	4.6
240 + 242	10.8	15.3	6.9	147.0	−33.5	14.0	5.9
250 + 252	5.8	11.6	4.1	312.0	−42.8	24.9	5.9
264 + 266	1.6	6.8	1.3	121.6	−44.1	39.4	4.5
276 + 278	4.6	9.9	3.3	256.2	−24.8	27.4	4.3
288 + 290	0.6	6.0	0.5	75.6	−33.8	45.7	6.1
300 + 302	2.5	6.5	1.9	122.7	−72.1	31.6	3.5
316	0.8	3.6	0.7	25.6	−15.7	41.2	3.0
326 + 328	1.2	5.4	1.1	51.2	−23.9	40.9	5.9

All results are in units of ng m^{-3} . The statistical analysis was carried out for the 4-point smoothed 4-min data. Note that the detection limit for the 4-min data is approx 4 times larger than for 1-h data. The minimum values sometimes exceed the 4-min detection limits, due to non-Gaussian effects on the noise distribution.

that the Q-AMS is capable of measuring particulate PAH in ambient air.

If PAHs were not present in concentrations detectable with the Q-AMS, the application of the subtraction procedure should produce as many negative as positive concentrations, due to the dominant influence of noise in that situation. The fraction of negative APAH concentrations is inversely proportional to the APAH concentration (Figure SI-3), and is only large for those PAHs whose average concentrations are similar to their detection limits (Table 2 above). The total PAH (sum of all MWs) and the modified total PAH (sum of PAHs with molecular weights 202, 226 + 228, 250 + 252, 276 + 278 and 300 + 302) contain only 9% or less negative signals. The modified total (APAH^{*}) is used for the comparison with the results of PAS measurements (SPAH). It excludes PAH signals for APAHs with MWs of 216, 240 + 242, 264 + 266, 288 + 290, 316 and 326 + 328 as the photoionization instrument's calibration does not account for such species [18]. Note that the negative concentrations need to be averaged with the positive ones in the calculation of PAH concentrations, as otherwise a positive bias would be introduced. The dominance of positive concentrations indicates that there is excess signal above the non-PAH organic background at the characteristic fragment ions of the PAHs, and thus that the Q-AMS is capable of detecting these species in ambient air, even in the presence of a non-PAH organic background. The current Q-AMS detection technique is not capable of distinguishing among various PAH isomers that have the same molecular weight. The new ToF-AMS instruments should be able to obtain additional information on ambient PAHs. The C-ToF-AMS will allow for the subtraction method to be applied to the size distribution data, while the high-resolution ToF-AMS may allow to directly quantify PAH and non-PAH signal for individual m/z values.

Fig. 3 illustrates this subtraction method by showing the average mass spectra of PAHs on top of the non-PAH organic background during different periods of MCMA-2003. Fig. 3a shows the average mass spectrum for the period with the highest PAH mass concentrations measured during this study. The PAH peaks are distinctively above the non-PAH organic baseline

signals. The early morning (5–9 a.m.) average spectrum for the whole campaign (Fig. 3b) indicates that the high PAH concentrations during the morning rush hour cause distinct PAH signals to appear above the non-PAH organic baseline signal. In contrast, during the lowest PAH concentration periods (2 p.m.–6 p.m., Fig. 3c), the estimated PAH signal is small, with an intensity similar to or smaller than the estimated non-PAH organic at the main PAH m/z values. Note that, even though the relative uncertainty in the reported PAH concentration is significant in this later case, the Q-AMS is still providing valuable negative information: the concentration of particle-phase PAHs is small, which is consistent with the SPAH and FPAH data discussed later in the text. Fig. 3d shows the average mass spectrum for the whole MCMA-2003 at CENICA.

Particle-associated PAH species determined by GC–MS analyses to be present during the MCMA and that should be measurable with the Q-AMS are shown in Table 1. The APAH detection limits (DLs), average mass concentrations, fraction of negative numbers and other statistical parameters are given in Table 2. The APAH DLs were estimated as three times the standard deviation of the reported concentrations in several periods when the Q-AMS was sampling ambient air through a filter. One hour DLs are in the range 3–6 ng m^{-3} for the individual groups of APAHs with the same MW, and 15 and 8 ng m^{-3} for the total (APAH) and modified total (APAH^{*}) concentrations, respectively.

3.1.4. Detailed comparison of the groups of peaks around molecular ions

In order to further examine the performance of the Q-AMS PAH subtraction procedure, we have compared the group of peaks around the molecular ion for PAHs in the NIST database (selecting those reported by GC–MS for MCMA-2003, Table 1), with those from Q-AMS analysis of pure laboratory particles and with the ambient Q-AMS mass spectra (after subtraction of non-PAH background as described in Section 3.1.2) in Figures SI-4 and SI-5 in the Supplementary Information. Note that PAHs of MWs other than those of the pure standards used here may also be present in the ambient spectra, as discussed

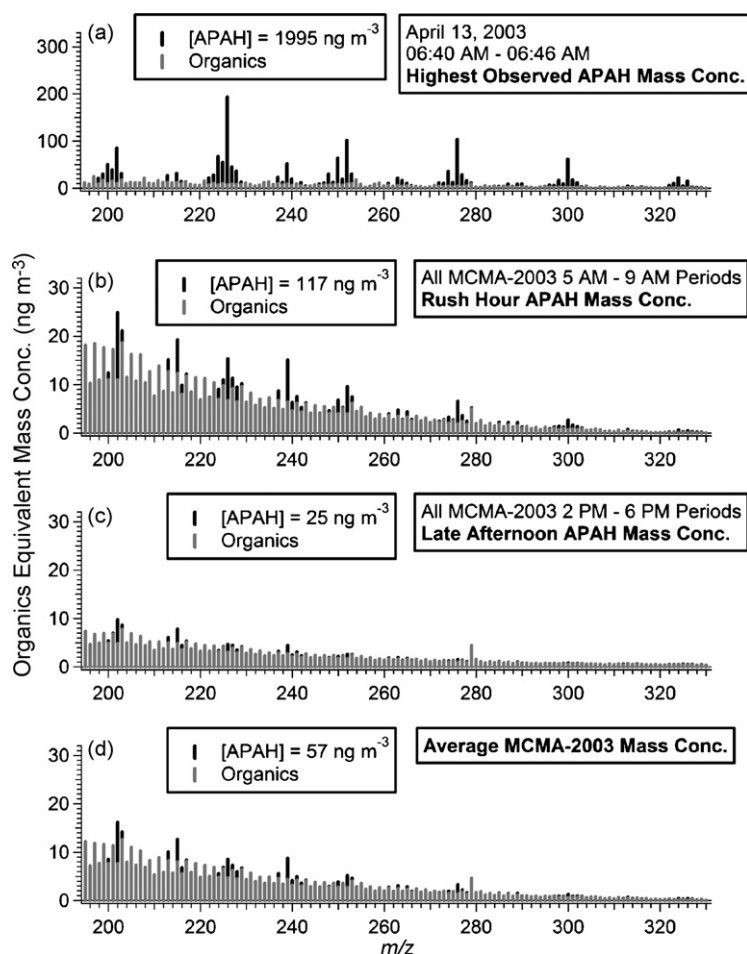


Fig. 3. Examples of the non-PAH organic signal subtraction method used with Q-AMS measurements to estimate PAH signal in ambient mass spectra. (a) shows PAH peaks above the non-PAH organic baseline signals for the average mass spectrum of the highest PAH mass concentrations measured during MCMA-2003 at CENICA, during April 13, 2003, from 6:40 a.m. to 6:46 a.m. (b and c) show the average mass spectra for selected time periods of MCMA-2003: (b) shows for all 5 a.m.–9 a.m. periods, corresponding to early morning rush hour (high PAH concentrations), and (c) for all 2 p.m.–6 p.m. periods, corresponding to late afternoons (which typically had the lowest PAH concentrations). (d) shows the CENICA average mass spectrum for the MCMA-2003.

below. For most spectra there seems to be a consistent pattern of the group of ion peaks around the molecular ion. The NIST database spectra of fluoranthene and pyrene in this region are very similar (Figure SI-4a). Normalized to the molecular ion at m/z 202, the ^{13}C isotope peaks are similar for all spectra. The $[\text{M} - \text{H}]$ and $[\text{M} - \text{H}_2]$ peaks are more abundant for all the Q-AMS pyrene laboratory spectra than those for the NIST database pyrene spectrum. This is consistent with the enhanced fragmentation in the AMS described above. Similar patterns are observed in Figures SI-4b–4d and SI-5a–5d for PAHs of other MWs. The peaks from ambient spectra are similar to those from the Q-AMS standards. The main exception to this pattern appears for PAHs of MW 252 (Figure SI-4c), where the Q-AMS PAH signals at m/z 250 are much higher for both ambient spectra and especially the flame spectrum. The Q-AMS spectrum of benzo[*e*]pyrene standard (shown in Figure SI-4c) does show greater fragmentation than the NIST database spectrum at m/z 250, but not to the degree seen in the ambient and especially the flame spectra. It is possible that PAHs of MW 250, such as corannulene or a dicyclopentapyrene, are present in the flame and ambient samples, which are not being accounted for in this comparison.

3.1.5. Quantification of Q-AMS PAH concentrations

This section describes the data and procedures needed to convert the Q-AMS PAH signals into mass concentrations. PAH fragments and multiply-charged ions will also be present at m/z values below 200, which we cannot quantify directly in ambient spectra with unit m/z resolution since they are buried in the significantly larger organic signals at lower m/z . Generally, the perturbation introduced by the PAH fragments into the mass spectrum at m/z values below 200 will be very small since on average the PAH mass concentration represents less than 1% of the ambient total organic mass concentration (during MCMA-2003 PAHs comprised 0.27% of the Q-AMS average organic mass conc.). The mass concentration of a species in the AMS is proportional to the sum of the signal at all of its ion fragments [23]. Thus, in order to account for the total PAH signal measured with the AMS we need to correct the PAH signal measured above m/z 200 with a factor to account for the signal contribution of the multiply charged ions and low m/z fragments. The quantification of the degree of PAH fragmentation (and doubly-charged ions) for NIST database and Q-AMS laboratory PAH spectra versus MW is given in Figure SI-6. We define the PAH frag-

mentation factor (FF) as the ratio of the total signal from a pure PAH summed for all m/z values, to the summed signal from the main group of peaks around the molecular ion. FF allows the estimation of the total PAH ion signals for ambient Q-AMS data for which only the main group of peaks are available. For the Q-AMS spectra of eight PAHs we obtain an average FF of $1.89 \pm 10\%$. Repeating this analysis for the NIST database spectra of the same eight PAHs (also shown in Figure SI-4), we obtain an average FF of $1.50 \pm 18\%$, indicating more fragmentation in the Q-AMS (as expected from the higher vaporization temperatures). Note that there is less scatter around the regression line for the Q-AMS data than for the NIST data, likely due to the use of a single instrument for the Q-AMS versus many different mass spectrometers for NIST database. There is a molecular weight dependence of fragmentation factor for both Q-AMS and NIST database spectra: the heavier the PAH, the more signal is accounted for by fragments and doubly-charged ions. Thus, we have used a different FF for each group of PAHs at a given MW, calculated as: $FF = (553.3 + 5.6 \times MW) \times 10^{-3}$, giving the range of PAH FFs of 1.69–2.40.

Besides this fragmentation correction, the relative ionization efficiency (RIE) with respect to nitrate is also needed to calculate mass concentrations from the AMS data [23,53]. We have used the value of 1.35 measured for pure pyrene particles in a recent Q-AMS laboratory calibration [19], and the results of laboratory calibration experiments of selected PAH standards with the same Q-AMS instrument used during MCMA-2003. The measured PAH RIEs are given in Figure SI-7. We used different RIEs for each group of PAHs at a given MW, calculated as: $PAH\ RIE = 0.12^* \times \sqrt{PAH\ MW}$, giving the range of PAH RIEs of 1.63–2.08. The square root dependence is expected due to the longer residence time of heavier PAHs in the ionization region. Marr et al. [18] used a constant FF of 1.77 and a constant RIE of 1.35 to obtain the AMS PAH mass concentrations. Applying different FFs and RIEs to each group of PAHs with the same MW decreases the mass concentration of total APAH by 17% when compared to those obtained by applying the constant FF and RIE values of 1.77 and 1.35, respectively.

3.1.6. Signal and uncertainty analysis

In order to estimate the average uncertainty introduced by the interference subtraction procedure for non-PAH organics, we analyzed the MS signals at the m/z values assigned to the PAHs and their signal to noise ratios (SNRs). Fig. 4a shows that the average estimated PAH fraction over the entire campaign, calculated as (estimated PAH signal)/(total signal) at each m/z , is $\sim 50\%$ for most molecular ion peaks. The average estimated non-PAH organic mass concentrations for all m/z values between 198 and 300 (Fig. 4a) shows a uniform downward trend (with the even/odd pattern described above) after subtraction of the estimated PAH signal. This indicates that the subtraction method used here works reasonably well, i.e., there is no indication of a significant positive or negative bias in the trends of the non-PAH organic spectrum after applying the subtraction procedure. The signal-to-noise analysis presented in Fig. 4b shows that the average signal at the PAH m/z values peaks is steadily declining as m/z increases. The noise decreases due to the decrease

in the ionic background in the Q-AMS with increasing m/z , albeit more slowly than the decrease in signal (approximately proportional to the square root of the signal due to Poisson ion counting statistics, and also influenced by electronic noise which does not depend on m/z). Thus, the SNR decreases significantly with increasing m/z , although it remains above the detection limit ($SNR = 3$) for all peaks for this long average of the whole campaign.

The uncertainties in the estimation of the non-PAH interference will be an important factor limiting the absolute precision and accuracy achievable by the Q-AMS for PAH detection. However, note that this is not a situation where we are subtracting two large numbers to produce a small number, in which case the precision of the small number would be poor. Rather the non-PAH organic background and the PAH concentrations are about equal on average for the m/z 's that contribute most of the PAH signal. The background subtraction method has lower uncertainty when (1) PAH concentrations are higher since SNR is higher; and (2) PAH signals are larger relative to the non-PAH organic signals, since then the subtraction is a small fraction of the total signal at the main PAH m/z values. We have estimated the uncertainty due to the subtraction procedure, based on the propagation of uncertainty from the estimated noise in each m/z (from Allan et al. [54]). The estimated average uncertainty due to the subtraction procedure for the total APAH is 27%. One hour uncertainties are in the range of 1.7 – $2.4\ ng\ m^{-3}$ for the individual groups of APAH with the same MW, and 7 and $5\ ng\ m^{-3}$ for the total and modified total APAH concentrations, respectively. The detailed description of the uncertainty calculation is given in Appendix 3.

We have also attempted to determine whether some expected PAH reaction products could produce a detectable signal in the Q-AMS. The products we considered are PAH-quinones (MW = single PAH + 30), hydroxy-PAH (MW = single PAH + 16), and finally selected nitro-PAHs (MW = 247, 273, and 297). The signals from these species are expected to be very low, due to the low concentrations of these PAH reaction products, which are expected to be ~ 100 times smaller than PAH levels. Thus, on average we would expect these species to contribute only $\sim 1\%$ of the total Q-AMS signal at the m/z 's of their molecular ions. For example, the range of mass concentrations measured during MCMA-2003 by GC-MS analysis of filter samples for 2-nitrofluoranthene, 2-nitropyrene and 1-nitropyrene were, 7–185, 1–114 and 1–23 $pg\ m^{-3}$, respectively [Arey, Reisen and Bethel, unpublished data]. The non-PAH organic signal at those peaks would be expected to contribute $\sim 99\%$ of the signal. Indeed these m/z 's do not stick out from the neighboring peaks. We conclude that the Q-AMS was not capable of measuring these PAH reaction products in ambient air during MCMA-2003.

In summary the Q-AMS should be capable of providing a quantitative measurement of PAH mass concentrations in the ambient aerosol, limited by the uncertainties in the subtraction of the interference of non-PAH organics ($\pm 27\%$, 1σ), in the fraction of low m/z fragments and multiply charged ions ($\pm 10\%$, 1σ), in the ionization efficiency relative to nitrate ($\pm 19\%$, 1σ) and in the AMS particle collection efficiency ($+10\%/ -30\%$ total uncertainty) [36]. Adding these independent sources of uncer-

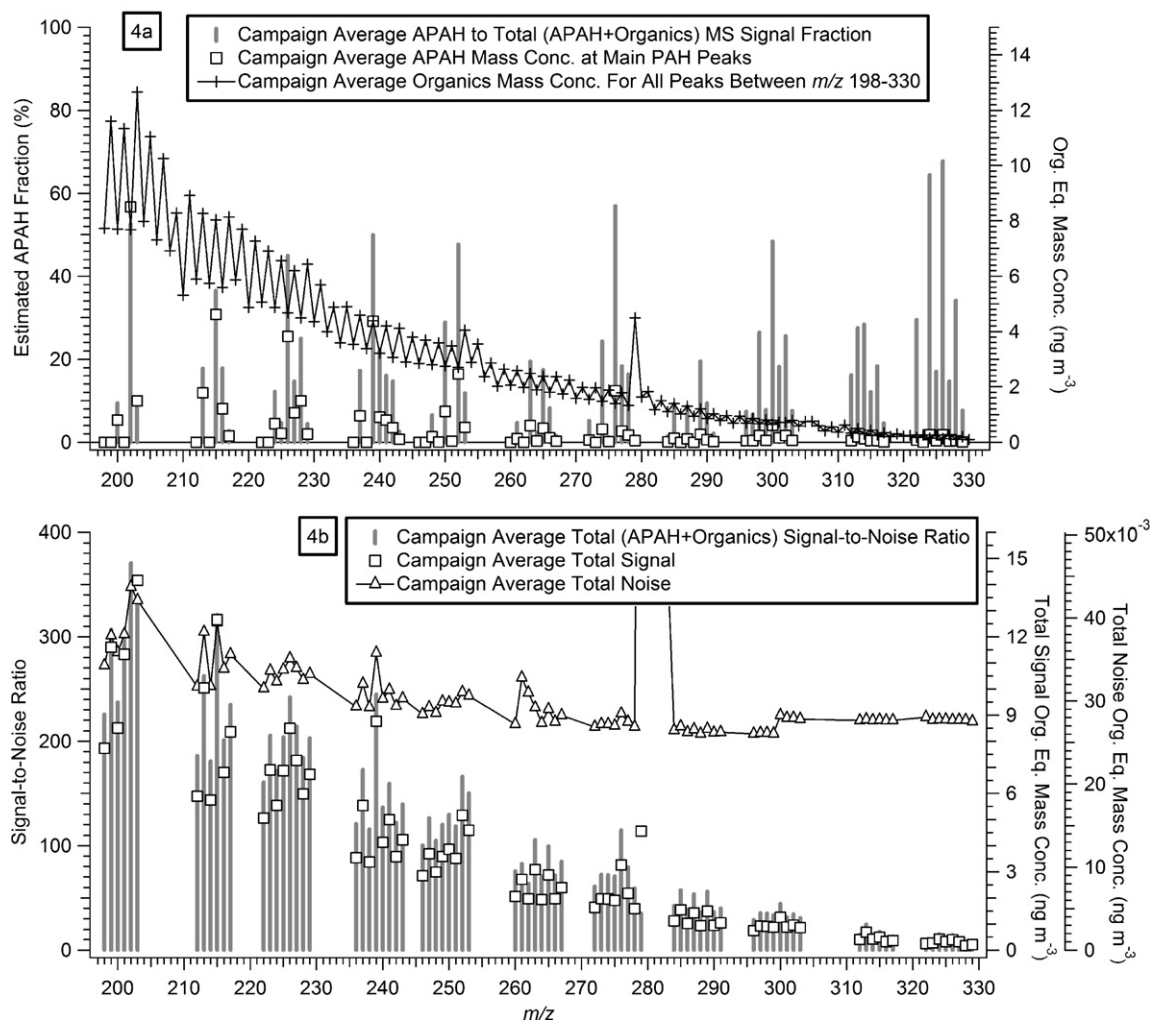


Fig. 4. Analysis of the average MCMA-2003 PAH and non-PAH signals for ions above m/z 198. (a) shows the estimated PAH fraction as (estimated PAH signal)/(total signal), where total signal refers to the sum of PAH + non-PAH organic signals at the each m/z . Also plotted are the average MCMA-2003 non-PAH organics mass concentrations for all m/z values between 198 and 300. (b) shows the average Q-AMS MCMA-2003 total signal, noise, and signal-to-noise ratio at the PAH m/z values. Signal at m/z 279 likely originates from phthalates.

tainty in quadrature we obtain total uncertainty bounds of +35% and –38% (1σ) for the APAH concentrations.

3.2. Q-AMS measurements of particle-bound PAHs during MCMA-2003

Fig. 5 shows the time series of the PAS SPAH and modified AMS APAH (APAH*, see Section 3.1.3.) measured during MCMA-2003. As described in detail by Marr et al. [18], the APAH* and SPAH are clearly correlated and show not only large diurnal variations but also short-term spikes. However the APAH* and SPAH absolute values are not the same: the APAH* mass concentrations are often higher than SPAH during periods with lower PAH mass loadings. During the traffic emission periods in the mornings, the relative difference between APAH* and SPAH values becomes smaller or vanishes altogether. See Marr et al. [18] for a more detailed comparison and a discussion of the observed differences and their possible causes.

During MCMA-2003, the largest particle-phase PAH loadings are observed during periods dominated by traffic emissions

in the mornings. Thus, PAHs should be correlated with other combustion emissions such as CO, NO_x, black carbon and hydrocarbon-like organic aerosols (HOA). The AMS can measure total organic aerosol mass concentrations, which compare well with organic carbon concentrations determined with thermal-optical OC analyzers [27,55]. A procedure has recently been demonstrated to extract the concentrations of hydrocarbon-like organic aerosols (HOA) and oxygenated organic aerosols (OOA) from AMS data in urban areas [46]. HOA are named after their fragmentation patterns, which are similar to those of hydrocarbons, and in urban areas correlate well with combustion tracers such as CO, NO_x, and EC [56]. OOA spectra are indicative of significant oxygen content and at least some of the time they appear to be secondary organic aerosol (SOA) [56,57].

Ambient pollutant ratios have been used for many years in air pollution research as a way to summarize observed relationships, compare different locations, and evaluate emissions models [e.g., 58]. Since combustion sources are clearly an important source of PAHs in Mexico City [18,59], the ratios

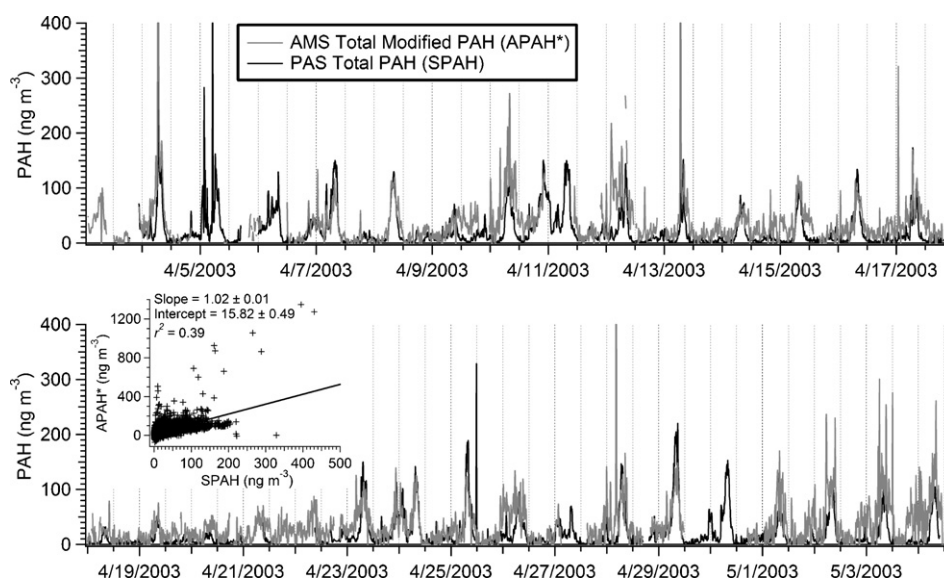


Fig. 5. Time series of AMS total modified APAH (APAHH*, sum of APAH with molecular weights 202, 226 + 228, 250 + 252, 276 + 278 and 300 + 302) and specific PAH (SPAHH) measurements during MCMA-2003. The correlation between APAHH* and SPAHH is shown in a scatter plot (inner panel).

of their ambient concentrations to the main combustion tracer species (HOA, black carbon, CO and NO_x) represent the average behavior of the sources in Mexico City and can be used to compare to other locations and/or laboratory experiments in the future. Thus, we have studied the correlation between APAH and the tracers of traffic emissions during MCMA-2003. Fig. 6a–d show the scatter plots between APAH and primary emissions markers, indicating a significant correlation as expected. The slopes of the regression lines with the intercept fixed to zero (except for CO where the intercept is set to a background value of 100 ppbv), that represent the average emission ratios of each pollutant pair, between APAH and HOA, black carbon, CO and NO_x are 7.1 ng μg⁻¹, 13.8 ng μg⁻¹, 35.1 ng m⁻³ ppmv⁻¹ and 0.79 ng m⁻³ ppbv⁻¹, respectively.

The total AMS PAH concentration and its contributing PAH MW groups have clear diurnal cycles, as illustrated in Fig. 7. Three groups of APAHs were chosen as representative for PAHs with low, medium and high MW. The diurnal cycles of most APAH resemble the CO diurnal pattern, while the APAHs of MWs 202 and 216 resemble more the diurnal pattern of HOA. These measurements might be capturing a real difference in the time profiles of the PAHs of different MWs. It is known that different sources can emit different PAH mixtures and have different diurnal activity patterns. For example gasoline vehicles and diesel trucks have different diurnal activity patterns [60] and PAH emission profiles [61,62], with gasoline vehicles emitting a larger fraction of high molecular weight PAHs, while diesels emit a larger fraction of the lower molecular weight

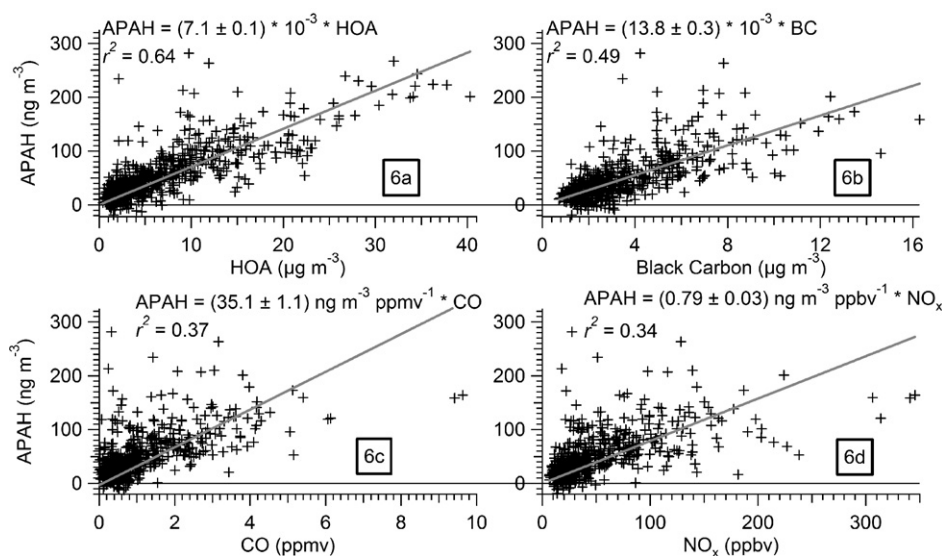


Fig. 6. Scatter plots between APAH and primary emissions markers for the whole MCMA-2003 1 hour averaged data (except for 2 outliers removed from the total of 656 points). The slopes of the regression line, forced through zero for all the correlations (except for CO where it is forced at a background level of 100 ppbv), between APAH and HOA, black carbon, CO and NO_x are indicative of emission ratios of APAH to other primary pollutants.

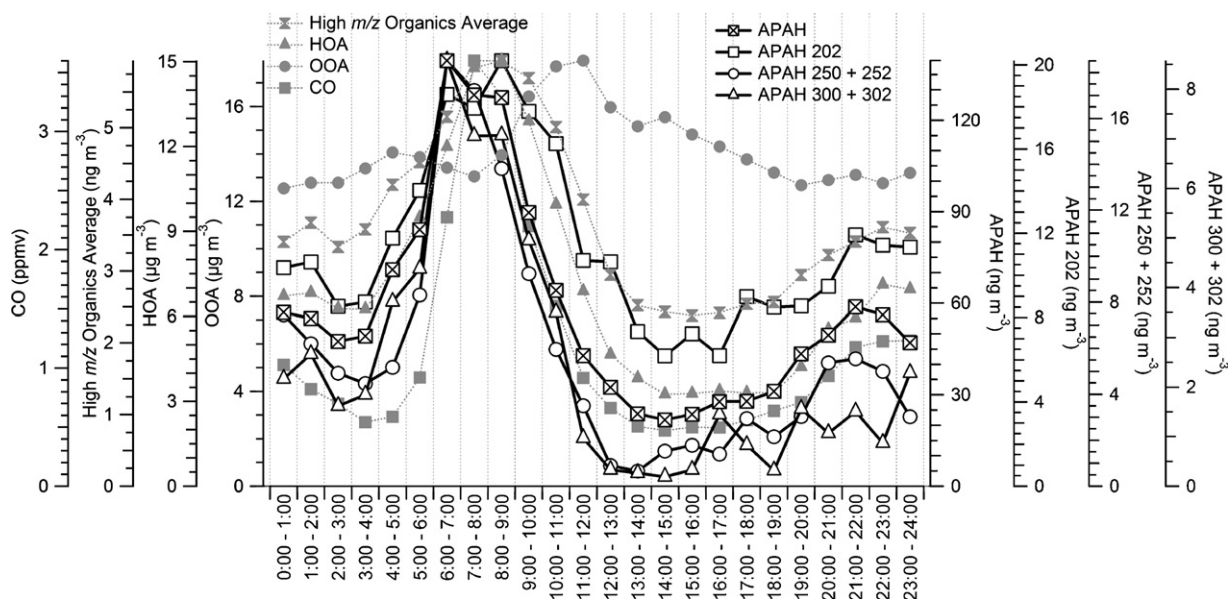


Fig. 7. Diurnal cycles of selected individual PAH MW groups, AMS organic species and CO during MCMA-2003. APAHs with MWs 202, 250 + 252 and 300 + 302 were chosen as representative for PAHs with low, medium and high MW. Organic signals from the following m/z values are added together to produce the “high m/z organics” data: 209, 219, 232, 244, 257, 269, 282, and 294. These were chosen for their very low likelihood to contain PAH fragments.

PAHs. Consistent with different gasoline and diesel activity patterns, benzo[ghi]perylene (a marker of gasoline vehicles) was high in the early morning and the ratio of methylphenanthrene/phenanthrene (a marker of diesel emissions) increased in the day [18]. While benzo[ghi]perylene can also originate from fires and other sources, vehicles are expected to be the dominant source [63–69], especially given that the timing of peak concentrations corresponds to the morning rush hour period in Mexico City.

3.3. Comparison of APAH to FPAH measurements

3.3.1. Spectral and concentration intercomparisons

Listed in Table 1 are the concentrations of specific FPAH quantified by GC–MS in the 7–11 a.m. morning filter sample

from April 29, 2003. The most abundant PAH observed was benzo[ghi]perylene, a marker of gasoline vehicle emissions [18]. Based on these measured concentrations for the filter and summing all isomers, the most abundant ion peaks expected in the AMS spectra would be m/z 276 and m/z 252, followed closely by m/z 228 and m/z 226. Each of these ion peaks is indeed present in the Q-AMS spectra. Fig. 8 shows the comparison of a reconstructed “FPAH Total PAH Spectrum” (see figure caption for details) and Q-AMS PAH mass spectra for this period. The FPAH Spectrum is presented as the sum of filter (black) plus a fraction of the PUF signal estimated from partitioning theory [51] (dashed). One possible explanation for the differences in measured individual FPAH and APAH, discussed in more detail throughout this section, might be that some filter-collected PAH are volatilizing off the filter during collection

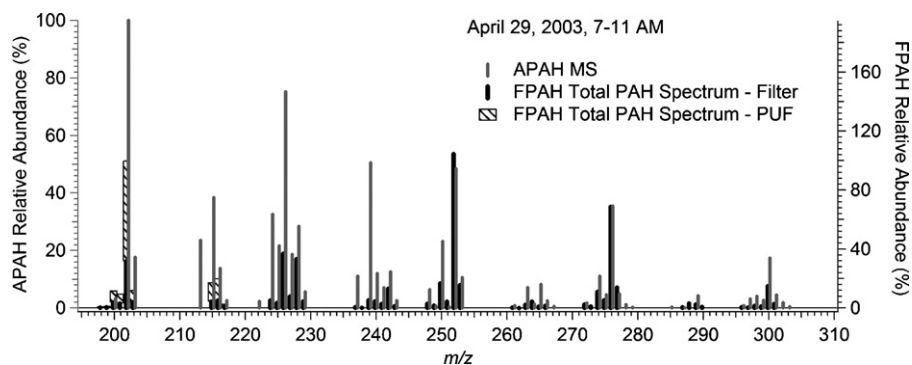


Fig. 8. Comparison of FPAH Total PAH Spectrum and Q-AMS PAH (APAH) mass spectra for April 29, 2003 from 7 to 11 a.m. The FPAH Total PAH Spectrum was constructed from a total ion current (scanning mode) analysis of the PAH-containing HPLC fraction of the ambient filter extract. Selected ion chromatograms were made for the ions shown, the GC peaks were integrated and the areas from the peaks attributed to the PAHs listed in Table 1 were summed. The FPAH Total PAH Spectrum is presented as the sum of filter (black) and PUF (dashed). The PUF data are available for FPAHs with molecular weight 202 and 216. The peak at m/z 202 for both spectra is set at 100%. Both spectra are scaled to the same height of PAH ions at m/z value 276 since these groups show good agreement in quantitative comparisons (see Fig. 9e). Note that the quantifications listed in Table 1 were made based on the addition of deuterated-PAH internal standards which would account for differences in behavior of the individual PAHs during the sample preparation and also differences in response in the GC/MS analysis.

and are being collected on the downstream PUF plugs, especially for more volatile, low MW PAHs such as ones with MW 202 and 216. Thus, in order to estimate the contribution of FPAHs with MW 202 and 216 to the FPAH Total Spectrum we have used partitioning theory [51] and applied it to the sum of filter + PUF FPAH mass concentrations measured in the field. We used the average temperature (19 °C) and the average organic mass measured ($35 \mu\text{g m}^{-3}$) at the time of sampling and an assumed activity coefficient of 1. The calculated percent of particle-phase partitioning for pyrene (MW = 202) and 2,3-benzofluorene (MW = 216) is 49% and 96%, respectively. It is obvious from Table 1 that the majority of the MW 202 and 216 species were measured on the PUFs, confirming a volatilization artifact. The PUF data (dashed) in Fig. 8 are thus calculated as the FPAHs with MW 202 and 216 that would be in the particle-phase in the atmosphere, but have been blown to the PUF plugs (as opposed to PAH species with MW 202 and 216 that would anyhow be present in the gas phase). There is a correlation between the two spectra with an r^2 of 0.64. The correlation between the same FPAH Total Spectrum and the unprocessed Q-AMS ambient 7 a.m.–11 a.m. data (PAH + non-PAH organics) results in a significantly lower r^2 of 0.23. We have normalized the spectra so that PAH ions at 276 are at the same height, since these groups show good agreement in quantitative comparisons (see below). The Q-AMS PAH spectrum shows higher relative abundance of ions attributed to PAHs with MWs 216, 226, 240, 250 and 264 + 266. It should be noted, however, that the [M – H] base peaks at m/z 215 and 239 are higher, relative to the observed molecular ions, than expected, for example, the Q-AMS spectrum of 2,3-benzofluorene in Fig. 1c shows m/z 215 as the base peak and m/z 216 at 70% relative abundance. All of those o-PAHs have a non-aromatic part in the molecule. Thus, they will be more reactive and prone to filter reactions, such as ozone oxidation, and as described in detail below. It also shows higher signal at MW 202 for the AMS, as discussed below.

We now present comparisons for all points in time for which both APAH and FPAH data exist. To properly compare PAH measured by the two techniques, we have averaged the APAH data onto the four FPAH filter sampling time periods. The comparison of Q-AMS APAH versus filter-collected FPAH, shown in Fig. 9 and Figure SI-8, reveals different results for the different PAH groups. There are only four filter samples that overlap with Q-AMS data. Comparison of PAH groups with MWs of 202 ($r^2 = 0.74$), 226 + 228 ($r^2 = 0.99$), 250 + 252 ($r^2 = 0.96$), and 276 + 278 ($r^2 = 0.80$) in Fig. 9 reveals good correlation; on the other hand, the correlation in individual PAH MW groups is lower for PAHs with MWs 216 ($r^2 = 0.11$), 240 + 242 ($r^2 = 0.46$) and 300 + 302 ($r^2 = 0.63$). Although for all PAH MW groups APAH and FPAH mass concentrations are of the same order, the ratios of the concentrations reported by the two techniques vary significantly, as suggested by the previous comparison in Fig. 8. For example, while the average measured APAH with MW of 226 + 228 and 250 + 252 are both highly correlated to the FPAH with the same molecular weight, the slopes of the regressions are significantly different. All the Q-AMS mass spectra averaged for the FPAH filter-sampling periods are given in the Figure SI-9. Q-AMS APAH measurements tend to be larger than the FPAH

of MW 252 and smaller, while the reported concentrations are similar for those of MW 276 and 300. Some of these discrepancies may be explained by reaction of some PAHs in the filters as described below.

3.3.2. Interpretation of the intercomparisons

In the FPAH sampling set-up, there were two polyurethane foam plugs in series beneath the filter and no attempt was made to remove ozone prior to sampling. To investigate the extent of possible volatilization of more volatile, low MW PAHs (MW 202 and 216) from the filter to the downstream PUF plugs during PAH filter-collection, we have also compared in Fig. 9b and Figure SI-8a the total measured FPAH with MW 202 and 216, respectively, as the sum of FPAH (filter + PUF). This procedure might be over-estimating the particulate PAHs, but all of them should be captured, and an upper limit (filter + PUF) and a lower limit (filter-only) can be compared. Finally, in order to obtain the best estimate of the contribution of FPAHs with MW 202 and 216 to the total particulate PAH mass loadings we have used partitioning theory (as described above) and applied it to the measured sum of filter + PUF FPAH. The calculated percent of particle-phase partitioning for pyrene (MW = 202) and 2,3-benzofluorene (MW = 216) is in the range of 20–49% and 87–96%, respectively. The FPAH filter + PUF total is closer to APAH values in both cases. These results indicate that, especially for the MW 202 PAHs, volatilization of PAHs from filters could account for some of the discrepancy between APAH and FPAH.

Another potential source of differences between these two measurements is chemical degradation of PAHs in/on the filters. Significant degradation, beyond what occurs in the atmosphere and would be common to both the APAH and FPAH, may occur during filter sampling and may reduce the measured concentrations of some FPAHs by a factor of 2 or more [70,71]. The extent of degradation during filter sampling will depend upon the concentration of atmospheric oxidants such as ozone, the length of the sampling period, and the reactivity of the individual PAHs. In order to estimate the degree of possible FPAH degradation during MCMA-2003 filter sampling we calculated the average ozone concentrations for all the FPAH sampling periods and applied a degradation estimation method developed by Schauer et al. [70] to FPAH. The results of it are presented in Fig. 9 as the FPAH positive error bars. Reactions in the filters may explain a significant fraction of the differences between FPAH and APAH. For the PAHs with MW 216, 226 + 228, and 240 + 242 the FPAH degradation as estimated with the method of Schauer et al. [70] cannot account for all the difference present.

A possible explanation for the remaining discrepancies is the presence of significant concentrations of individual PAH of higher reactivity than those captured in the treatment of Schauer et al. [70]. Kalberer et al. [11] report that o-PAHs degrade faster in the atmosphere than fully benzenoid PAHs, which may explain the larger discrepancies for 216 and 240 + 242.

By analogy with acenaphthylene [72], PAHs with cyclopenta-fused rings containing a double bond will be very reactive with ozone. Such reactive PAHs would include acephenanthrylene, cyclopenta[*cd*]pyrene and dicyclopenta[*cd,mn*]pyrene (see

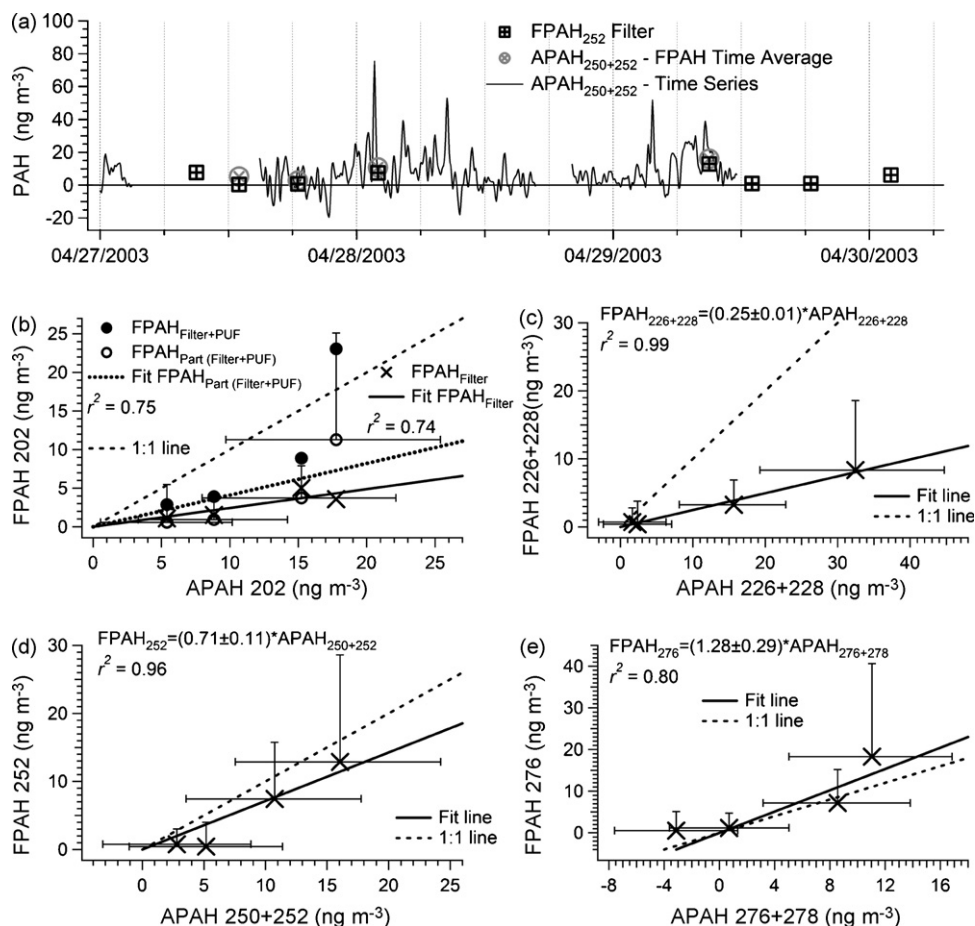


Fig. 9. Comparisons of selected individual FPAH and APAH. The mass concentrations time series is shown for the measured FPAH with MW 252 (all the FPAH mentioned in the text are also given in Table 2) and APAH with MW of 250 + 252. The scatter plots show correlations between FPAH and APAH with molecular weights of 202, 226 + 228, 250 + 252 and 276 + 278 (note that for the comparison of PAHs with main MW 252 and 276, we are comparing FPAHs with MW 252 and 276 to APAHs with MW 250 + 252 and 276 + 278, respectively). For the FPAH with molecular weight 202, two types of samples are shown: FPAH samples collected on filter (cross) and the sum of FPAH samples collected on filter + PUF (circle), both with eight data points. There are only four APAH points that overlap with filter and PUF samples. For the comparison of PAHs with MW 202 filter and PUF samples are represented in two ways: full circles show the sum of filter + PUF mass concentration as collected in the field, and empty circles show the results of applying the partitioning theory [51] and the average MCMA-2003 conditions for FPAH filter collection periods to the sum of filter + PUF mass concentrations. The line equations for the comparisons of PAHs with MW 202 are given here, due to the busy panel. Filter FPAH data (crosses): $\text{FPAH}_{202} = (0.24 \pm 0.04) \times \text{APAH}_{202}$; Partitioned filter + PUF data (empty circles): $\text{FPAH}_{202} = (0.41 \pm 0.13) \times \text{APAH}_{202}$. All the regression lines have the intercept forced through zero.

Table 1 for structures). Rapid degradation of acephenanthrylene would contribute to the differences observed at m/z 202. In the spectra comparison in Fig. 8, the Q-AMS m/z 226 and m/z 250 ions are very elevated over what would be expected based on the GC–MS FPAH analysis. The ion peak at m/z 226 will contain contributions from both the molecular ions of cyclopenta[cd]pyrene and benzo[ghi]fluoranthene (MW = 226) and from the $[M - H_2]$ ions from benz[a]anthracene, chrysene and triphenylene (MW = 228). So there are two possible explanations for the high m/z 226 and m/z 250 peaks: (1) higher $[M - H_2]$ fragmentation in Q-AMS relative to the standard GC–MS EI system used for the FPAH analysis, or (2) PAHs of MW 226 and 250 were present in the ambient particles, but degraded during the FPAH sampling. Although the Q-AMS spectra shown in Fig. 1 and the Supplemental Information do show enhanced $[M - H_2]$ peaks in the Q-AMS relative to the NIST spectra, the large differences seen in Fig. 8 clearly support the second explanation.

Based upon the GC–MS data, the concentrations of the MW 228 species and the MW 226 species were about equal ($\sim 4 \text{ ng m}^{-3}$) for the morning sample on April 29, 2003 (Table 1 and Fig. 8). Cyclopenta[cd]pyrene was slightly higher than benzo[ghi]fluoranthene in this morning sample, but generally the relative abundances were reversed, especially in the afternoon samples when ozone was elevated [73]. As noted above, the double bond in the cyclopenta-fused ring of cyclopenta[cd]pyrene is expected to be very reactive, and rapid decay of cyclopenta[cd]pyrene in the atmosphere has been reported [74,75]. As suggested from the propane flame spectrum shown here (Fig. 2), certain flames contain abundant cyclopenta[cd]pyrene [76,77]. It seems likely, therefore, that more of this very labile compound was present in the ambient air than was measured in the FPAH sample collected over several hours and that, at least in the MCMA-2003, cyclopenta[cd]pyrene may be more abundant than the MW 228 PAH species. If confirmed, this is an important finding because

cyclopenta[*cd*]pyrene has been shown to contribute significantly to the human cell mutagenicity of ambient particles [4,78]. Furthermore, cyclopenta[*cd*]pyrene is carcinogenic in animal studies and has been classified as a “probable human carcinogen” at a recent IARC evaluation [5].

While cyclopenta[*cd*]pyrene has previously been reported in ambient samples, it is generally significantly less abundant than the MW 228 species [79,80], and to our knowledge no molecular weight 250 species has been reported in ambient samples. Molecular weight 250 species were reported in fuel-rich ethene flames [81], and Lafleur et al. [82] identified three dicyclopentapyrenes along with corannulene in “fullerene-deficient” flames. In “fullerene-forming” flames, such as benzene flames, corannulene was the only MW 250 PAH observed and its concentration was less than the MW 252 species observed [82]. GC–MS analysis of the April 29, 2003 morning filter sample showed a single very small MW 250 peak, which based on its elution order relative to the more abundant MW 252 species [82] is assigned to corannulene. So once again, the Q-AMS may be detecting very labile compounds, namely dicyclopentapyrenes, which are not detected in the filter samples.

It will be important to determine whether these cyclopenta-fused compounds are unique to the MCMA or if they are more universally distributed, but degraded during filter sampling. It should be noted that a marker of plastics combustion, 1,3,5-triphenylbenzene [83] was found in the MCMA FPAH samples, suggesting that although traffic is a dominant source

of PAHs in the MCMA, uncontrolled burning also makes a significant contribution [18]. While benzo[*a*]pyrene is undoubtedly a PAH subject to degradation by ozone or other oxidants [70,71], the isomeric benzo[*k*]fluoranthenes and benzo[*e*]pyrene are less reactive and the MW 252 species, as well as the MW 276 species show reasonable agreement between the FPAH and the APAH.

In summary, the comparisons show agreement for some PAH groups and higher APAH than FPAH concentrations for others. Degradation of the filter samples due to reaction with atmospheric oxidants, and to a lesser extent volatilization of the lighter FPAHs, may account for most of the differences. Further laboratory and field intercomparisons are needed in order to clarify whether reaction can account for all the observed disagreements, including filter sampling for short times and/or with a denuder to remove ozone. Additionally, the *m/z* 215 and *m/z* 239 ambient signals need to be verified as signals for PAHs of MW 216 and 240 with the high-resolution ToF-AMS.

3.4. Estimated size distributions of PAHs during MCMA-2003

The measurement of PAH size distributions is of interest as it can provide insights into the sources and microphysical processes of these species [e.g., 84]. One advantage of the AMS PAH measurements is that the AMS can also provide the size distributions of individual *m/z* ions with high time resolution,

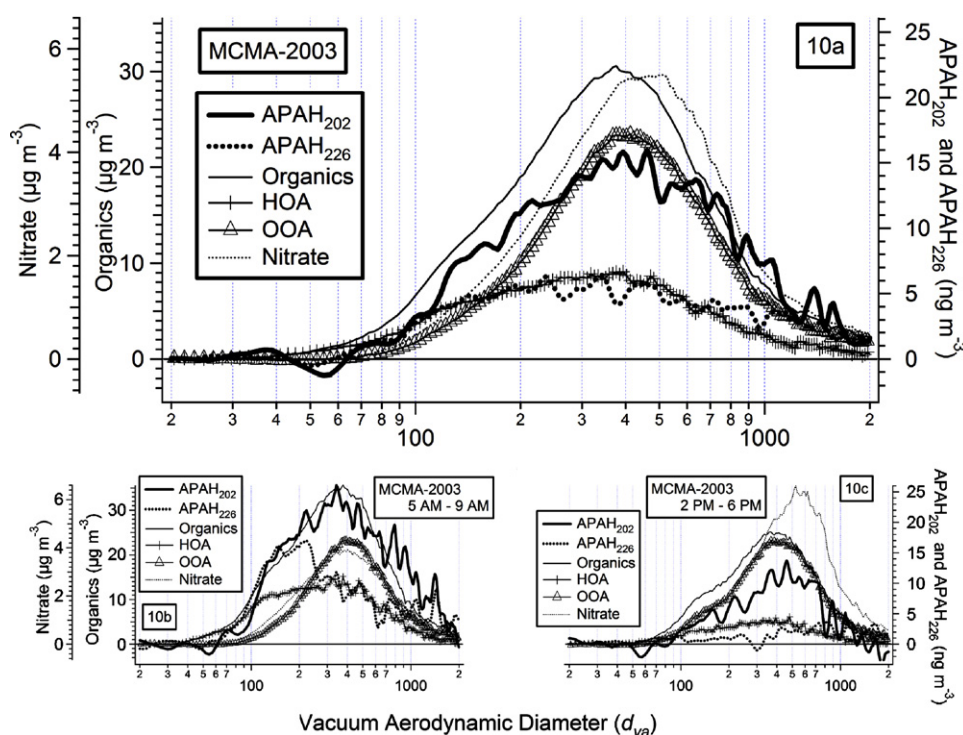


Fig. 10. MCMA-2003 average size distributions of APAHs with molecular weights 202 and 226 are compared with Q-AMS-measured total organics, HOA, OOA, and nitrate for the following time periods: (a) shows the average MCMA-2003 size distributions, (b) shows all MCMA-2003 5 a.m.–9 a.m. periods, and (c) shows all MCMA-2003 2 p.m.–6 p.m. periods. Selected *m/z*'s 202 and 226 were scanned from April 9, 2003 at 11:10 p.m. All three panels in this Figure have the same axis ranges to facilitate their direct comparison.

which are not easily obtainable with the other two methods. However only a limited number of m/z values can be scanned in the particle time-of-flight (PToF) mode of the Q-AMS used in Mexico City, as there is a tradeoff between this number and the duty cycle/signal-to-noise of the selected m/z 's [23]. During MCMA-2003 two m/z 's corresponding to PAH molecular ions were scanned: m/z 's 202 and 226. Note that in this case it is not possible to perform the interference subtraction procedure described above for the mass spectral signals, since the size distributions of the surrounding m/z 's are not available for this study. Thus, the recorded size distributions are an average of those from the PAHs and the non-PAH organics producing signals at the same m/z 's, in about 50/50 proportions. To determine the PAH-only size distribution, we have estimated and subtracted the size distribution of non-PAH organics at those two m/z 's. The HOA/OOA deconvolution procedure [46] was used to quantify the percent of the non-PAH organic signal at m/z 202 and 226 that is due to HOA and OOA. The non-PAH organic size distributions at m/z 202 and 226 were then estimated using the size distributions of HOA and OOA, weighed by the contributions of these two groups of species to each m/z .

The results of this procedure are shown in Fig. 10. Fig. 10a compares the MCMA-2003 average size distributions for PAHs with MWs 202 and 226, with those of total organics, hydrocarbon-like (HOA) and oxygenated (OOA) organic aerosols. Nitrate is also shown in order to represent the inorganic species, since most inorganic species have very similar size distributions to that of nitrate during MCMA-2003 [36]. The average size distributions of PAHs with MWs 202 and 226 are broad, with maxima between 300 and 400 nm. Fig. 10b and c show the comparison of the size distributions of PAHs with MWs 202 and 226 averaged over selected time periods during each day of MCMA-2003. The two periods selected are from 5 a.m. to 9 a.m., corresponding to times when PAHs are intensely emitted during the rush hour and trapped by the relatively low boundary layer, and from 2 p.m. to 6 p.m., representative of the lowest PAH concentration periods. A noticeable difference is the higher concentration of PAHs with MW 202 and 226 in smaller particles (between 100 and 250 nm) during the early morning, which is expected since fresh traffic emission particles extend into low vacuum aerodynamic diameters (d_{va}) [56]. The early morning PAH size distributions resemble more HOA than OOA size distributions, indicating again that the PAH sources are more associated with the HOA sources. During afternoon times the distributions shift to larger diameters, which is observed for all species in the city, likely due to condensation of secondary species and coagulation [36]. The early morning size distributions of PAHs with MWs 202 and 226 have a different maximum: while PAHs with MW 202 peak around 350 nm, PAHs with MW 226 peak around 200 nm. This may be due to differences in the sources of these PAHs, as suggested by the differences in the diurnal cycles above.

4. Conclusions

This paper reports the quantification of PAHs in ambient air using a real-time aerosol mass spectrometer for the first time.

The Q-AMS spectra of pure PAH standards are similar to those in the NIST database, albeit with larger fragmentation. We have developed a quantification procedure, including a background subtraction method that allows us to remove the interferences from non-PAH organics on m/z values with PAH contributions. Multiple tests have been applied to the ambient data that confirm the ability of our method to separate the PAH signals from those of non-PAH species. Based on comparisons with laboratory Q-AMS and NIST database spectra of PAH standards, the Q-AMS is capable of measuring particulate PAH in ambient air, with an estimated uncertainty of +35% and –38%.

The time series of SPAH and total modified APAH (APAH*) measurements during MCMA-2003 are generally well correlated. Correlation between APAH and primary emissions markers is also observed. For the average of the whole MCMA-2003, the slopes of the regression lines, which are indicative of APAH emissions ratios, between APAH and HOA, black carbon, CO and NO_x are 7.1 ng μg^{-1} , 13.8 ng μg^{-1} , 35.1 ng m^{-3} ppmv⁻¹ and 0.79 ng m^{-3} ppbv⁻¹, respectively. The Q-AMS and filter+GC-MS measurements are compared in detail. The comparisons show agreement for some PAH groups and higher APAH than FPAH concentrations for others. Degradation of the filter samples due to reaction with atmospheric oxidants, and to a lesser extent volatilization of the lighter FPAHs, may account for most of the differences. This issue needs to be further explored by laboratory and additional field intercomparisons of the two techniques. Some of the discrepancies suggest the presence of highly reactive PAHs such as cyclopenta[cd]pyrene and dicyclopentapyrenes, which would be sampled by the Q-AMS but could be degraded in the filter sampler, and which would be important due to their potential health effects.

Acknowledgments

We are grateful to Dr. Rafael Ramos of RAMA for his help with Mexican customs, and Salvador Blanco and Felipe Angeles of CENICA for their help in setting up the instrumentation at CENICA. We thank Jay Slowik of Boston College and Megan Northway of Aerodyne for sharing their PAH lab data, Fabienne Reisen and Heidi Bethel of University of California at Riverside for their help with the FPAH, and James Allan (University of Manchester) and Frank Drewnick (Max Planck Institute) for AMS data analysis software. We also thank Lada Klaic (Northwestern Univ.) for drawing the PAH molecular structures. This project was funded by the NSF Atmospheric Chemistry Program (Grants ATM-0300748 and ATM-0528634), the Atmospheric Sciences Program of the US Department of Energy (BER, Grant DE-FG02-05ER63981), the US EPA (STAR grant RD-83216101-0) and an NSF CAREER Award to J.L. Jimenez (grant ATM-0449815). This research has not been subjected to the review of either funding agency and therefore does not necessarily reflect the views of the agencies and no official endorsement should be inferred. K. Dzepina is an Advanced Study Program (ASP) and Atmospheric Chemistry Division (ACD) National Center for Atmospheric Research Fellow. We also thank an anonymous reviewer for many useful suggestions.

Appendix A. Supplementary data

Supplementary data associated with this article can be found, in the online version, at [doi:10.1016/j.ijms.2007.01.010](https://doi.org/10.1016/j.ijms.2007.01.010).

References

- [1] M. Howsam, K.C. Jones, in: A.H. Neilson (Ed.), *The Handbook of Environmental Chemistry*, Springer-Verlag, Berlin, 1998, p. 137.
- [2] B.J. Finlayson-Pitts, J.N. Pitts Jr., *Chemistry of the Lower and Upper Atmosphere*, Academic Press, San Diego, 2000.
- [3] F. Wania, D. Mackay, *Environ. Sci. Technol.* 30 (1996) 390.
- [4] M.P. Hannigan, G.R. Cass, B.W. Penman, C.L. Crespi, A.L. Lafleur, W.F. Busby, W.G. Thilly, B.R.T. Simoneit, *Environ. Sci. Technol.* 32 (1998) 3502.
- [5] IARC: K. Straif, R. Baan, Y. Grosse, B. Secretan, F. El Ghissassi, V. Coglian, *Lancet Oncol.* 6 (2005) 931.
- [6] D.W. Dockery, C.A. Pope, X.P. Xu, J.D. Spengler, J.H. Ware, M.E. Fay, B.G. Ferris, F.E. Speizer, *N. Engl. J. Med.* 329 (1993) 1753.
- [7] W.E. Wilson, H.H. Suh, *J. Air Waste Manage. Assoc.* 47 (1997) 1238.
- [8] C.A. Pope, R.T. Burnett, M.J. Thun, E.E. Calle, D. Krewski, K. Ito, G.D. Thurston, *JAMA-J. Am. Med. Assoc.* 287 (2002) 1132.
- [9] C.A. Pope, *N. Engl. J. Med.* 351 (2004) 1132.
- [10] D.L. Poster, M.M. Schantz, L.C. Sander, S.A. Wise, *Anal. Bioanal. Chem.* 386 (2006) 859.
- [11] M. Kalberer, S. Henne, A.S.H. Prevot, M. Steinbacher, *Atmos. Environ.* 38 (2004) 6447.
- [12] C. Emmenegger, M. Kalberer, V. Samburova, R. Zenobi, *Environ. Sci. Technol.* 39 (2005) 4213.
- [13] P.T.A. Reilly, R.A. Gieray, W.B. Whitten, J.M. Ramsey, *J. Am. Chem. Soc.* 122 (2000) 11596.
- [14] R. Zimmermann, T. Ferge, M. Galli, R. Karlsson, *Rapid Commun. Mass Spectrom.* 17 (2003) 851.
- [15] D.S. Gross, M.E. Galli, P.J. Silva, S.H. Wood, D.Y. Liu, K.A. Prather, *Aerosol Sci. Technol.* 32 (2000) 152.
- [16] D.A. Sodeman, S.M. Toner, K.A. Prather, *Environ. Sci. Technol.* 39 (2005) 4569.
- [17] M.T. Spencer, L.G. Shields, D.A. Sodeman, S.M. Toner, K.A. Prather, *Atmos. Environ.* 40 (2006) 5224.
- [18] L.C. Marr, K. Dzepina, J.L. Jimenez, F. Riesen, H.L. Bethel, J. Arey, J.S. Gaffney, N.A. Marley, L.T. Molina, M.J. Molina, *Atmos. Chem. Phys.* 6 (2006) 1733.
- [19] J.G. Slowik, K. Stainken, P. Davidovits, L.R. Williams, J.T. Jayne, C.E. Kolb, D.R. Worsnop, Y. Rudich, P. DeCarlo, J.L. Jimenez, *Aerosol Sci. Technol.* 38 (2004) 1206.
- [20] R. Bahreini, M.D. Keywood, N.L. Ng, V. Varutbangkul, S. Gao, R.C. Flagan, J.H. Seinfeld, D.R. Worsnop, J.L. Jimenez, *Environ. Sci. Technol.* 39 (2005) 5674.
- [21] C.D. O'Dowd, J.L. Jimenez, R. Bahreini, R.C. Flagan, J.H. Seinfeld, M. Kulmala, L. Pirjola, T. Hoffmann, *Nature* 417 (2002) 632.
- [22] J.L. Jimenez, R. Bahreini, D.R. Cocker, H. Zhuang, V. Varutbangkul, R.C. Flagan, J.H. Seinfeld, C.D. O'Dowd, T. Hoffmann, *J. Geophys. Res. Atmos.* 108 (2003) 4318.
- [23] J.L. Jimenez, J.T. Jayne, Q. Shi, C.E. Kolb, D.R. Worsnop, I. Yourshaw, J.H. Seinfeld, R.C. Flagan, X. Zhang, K.A. Smith, J. Morris, P. Davidovits, *J. Geophys. Res. Atmos.* 108 (2003) 8425.
- [24] J.D. Allan, H. Coe, K.N. Bower, P.I. Williams, M.W. Gallagher, M.R. Alfarra, J.L. Jimenez, D.R. Worsnop, J.T. Jayne, M.R. Canagaratna, E. Nemitz, A.G. McDonald, *J. Geophys. Res. Atmos.* 108 (2003) 4091.
- [25] R. Bahreini, J.L. Jimenez, J. Wang, R.C. Flagan, J.H. Seinfeld, J.T. Jayne, D.R. Worsnop, *J. Geophys. Res. Atmos.* 108 (2003) 8645.
- [26] Q. Zhang, C.O. Stanier, M.C. Canagaratna, J.T. Jayne, D.R. Worsnop, S.N. Pandis, J.L. Jimenez, *Environ. Sci. Technol.* 38 (2004) 4797.
- [27] Q. Zhang, M.R. Canagaratna, J.T. Jayne, D.R. Worsnop, J.L. Jimenez, *J. Geophys. Res. Atmos.* 110 (2005) D07S09.
- [28] F. Drewnick, S.S. Hings, P.F. DeCarlo, J.T. Jayne, M. Gonin, K. Fuhrer, S. Weimer, J.L. Jimenez, K.L. Demerjian, S. Borrmann, D.R. Worsnop, *Aerosol Sci. Technol.* 39 (2005) 637.
- [29] P.F. DeCarlo, J.R. Kimmel, A. Trimborn, J.T. Jayne, A.C. Aiken, M. Gonin, K. Fuhrer, T. Horvath, K. Dockerty, D.R. Worsnop, J.L. Jimenez, *Anal. Chem.* 78 (2006) 8281, [doi:10.1021/ac061249n](https://doi.org/10.1021/ac061249n).
- [30] J.T. Jayne, D.C. Leard, X. Zhang, P. Davidovits, K.A. Smith, C.E. Kolb, D.R. Worsnop, *Aerosol Sci. Technol.* 33 (2000) 49.
- [31] P. Liu, P.J. Ziemann, D.B. Kittelson, P.H. McMurry, *Aerosol Sci. Technol.* 22 (1995) 293.
- [32] P. Liu, P.J. Ziemann, D.B. Kittelson, P.H. McMurry, *Aerosol Sci. Technol.* 22 (1995) 314.
- [33] X. Zhang, K.A. Smith, D.R. Worsnop, J.L. Jimenez, J.T. Jayne, C.E. Kolb, *Aerosol Sci. Technol.* 36 (2002) 617.
- [34] X. Zhang, K.A. Smith, D.R. Worsnop, J.L. Jimenez, J.T. Jayne, C.E. Kolb, J. Morris, P. Davidovits, *Aerosol Sci. Technol.* 38 (2004) 619.
- [35] P.F. DeCarlo, J.G. Slowik, D.R. Worsnop, P. Davidovits, J.L. Jimenez, *Aerosol Sci. Technol.* 38 (2004) 1185.
- [36] D. Salcedo, T.B. Onasch, K. Dzepina, M.R. Canagaratna, Q. Zhang, J.A. Huffman, P.F. DeCarlo, J.T. Jayne, P. Mortimer, D.R. Worsnop, C.E. Kolb, K.S. Johnson, B. Zuberi, L.C. Marr, R. Volkamer, L.T. Molina, M.J. Molina, B. Cardenas, R.M. Bernabé, C. Márquez, J.S. Gaffney, N.A. Marley, A. Laskin, V. Shutthanandan, Y. Xie, W. Brune, R. Leshner, T. Shirley, J.L. Jimenez, *Atmos. Chem. Phys.* 6 (2006) 925.
- [37] F.W. McLafferty, F. Turecek, *Interpretation of Mass Spectra*, University Science Books, Mill Valley, California, 1993.
- [38] M.L. Lee, M.V. Novotny, K.D. Bartle, *Analytical Chemistry of Polycyclic Aromatic Compounds*, Academic Press, New York, 1981.
- [39] S. Stein, Y. Mirokhin, D. Tchekhovskoi, G. Mallard, *The NIST Mass Spectral Search Program for the NIST/EPA/NIH Mass Spectral Library (Version 2.0); The Standard Reference Data Program of NIST*, 2001.
- [40] M.R. Alfarra, *Laboratory and Field Measurements of Organic Aerosols Using the Aerosol Mass Spectrometer*; Ph.D. Thesis, University of Manchester Institute of Science and Technology, 2004.
- [41] R.A. Dobbins, R.A. Fletcher, W. Lu, *Combust. Flame* 100 (1995) 301.
- [42] S.E. Stein, A. Fahr, *J. Phys. Chem.* 89 (1985) 3714.
- [43] R.A. Dobbins, R.A. Fletcher, H.-C. Chang, *Combust. Flame* 115 (1998) 285.
- [44] G. Grimmer, J. Jacob, K.-W. Naujack, G. Dettbarn, *Anal. Chem.* 55 (1983) 892.
- [45] A. Koganti, R. Singh, K. Rozett, N. Modi, L.S. Goldstein, T.A. Roy, F.J. Zhang, R.G. Harvey, E.H. Weyand, *Carcinogenesis* 21 (2000) 1601.
- [46] Q. Zhang, M.R. Alfarra, D.R. Worsnop, J.D. Allan, H. Coe, M.R. Canagaratna, J.L. Jimenez, *Environ. Sci. Technol.* 38 (2005) 4938.
- [47] H.J. Tobias, D.E. Beving, P.J. Ziemann, H. Sakurai, M. Zuk, P.H. McMurry, D. Zarling, R. Waytulonis, D.B. Kittelson, *Environ. Sci. Technol.* 35 (2001) 2233.
- [48] H. Sakurai, H.J. Tobias, K. Park, D. Zarling, S. Docherty, D.B. Kittelson, P.H. McMurry, P.J. Ziemann, *Atmos. Environ.* 37 (2003) 1199.
- [49] M.R. Canagaratna, J.T. Jayne, D.A. Ghertner, S. Herndon, Q. Shi, J.L. Jimenez, P.J. Silva, P. Williams, T. Lanni, F. Drewnick, K.L. Demerjian, C.E. Kolb, D.R. Worsnop, *Aerosol Sci. Technol.* 38 (2004) 555.
- [50] J.D. Allan, A.E. Delia, H. Coe, K.N. Bower, M.R. Alfarra, J.L. Jimenez, A.M. Middlebrook, F. Drewnick, T.B. Onasch, M.R. Canagaratna, J.T. Jayne, D.R. Worsnop, *J. Aerosol. Sci.* 35 (2004) 909.
- [51] J.H. Seinfeld, J.F. Pankow, *Annu. Rev. Phys. Chem.* 54 (2003) 121.
- [52] Y. Su, Y.D. Lei, F. Wania, M. Shoeib, T. Harner, *Environ. Sci. Technol.* 40 (2006) 3558.
- [53] M.R. Alfarra, H. Coe, J.D. Allan, K.N. Bower, H. Boudries, M.R. Canagaratna, J.L. Jimenez, J.T. Jayne, A. Garforth, S.M. Li, D.R. Worsnop, *Atmos. Environ.* 38 (2004) 5745.
- [54] J.D. Allan, J.L. Jimenez, H. Coe, K.N. Bower, P.I. Williams, D.R. Worsnop, *J. Geophys. Res. Atmos.* 108 (2003) 4090.
- [55] N. Takegawa, Y. Kondo, Y. Komazaki, Y. Miyazaki, T. Miyakawa, J.L. Jimenez, J.T. Jayne, D.R. Worsnop, J.D. Allan, R.J. Weber, *Aerosol Sci. Technol.* 39 (2005) 760.
- [56] Q. Zhang, D.R. Worsnop, M.R. Canagaratna, J.L. Jimenez, *Atmos. Chem. Phys.* 5 (2005) 3289.

- [57] R. Volkamer, J.L. Jimenez, F. San Martini, K. Dzepina, Q. Zhang, D. Salcedo, L.T. Molina, D.R. Worsnop, M.J. Molina, *Geophys. Res. Lett.* 33 (2006) L17811.
- [58] E.M. Fujita, B.E. Croes, C.L. Bennett, J. Air Waste Manage. Assoc. 42 (1992) 264.
- [59] L.C. Marr, L.A. Grogan, H. Wöhrnschimmel, L.T. Molina, M.J. Molina, T.J. Smith, E. Garshick, *Environ. Sci. Technol.* 38 (2004) 2584.
- [60] L.C. Marr, R.A. Harley, *Environ. Sci. Technol.* 36 (2002) 4099.
- [61] A.H. Miguel, T.W. Kirchstetter, R.A. Harley, *Environ. Sci. Technol.* 32 (1998) 450.
- [62] L.C. Marr, R.A. Harley, *Environ. Sci. Technol.* 33 (1999) 3091.
- [63] N.R. Khalili, P.A. Scheff, T.M. Holsen, *Atmos. Environ.* 29 (1995) 533.
- [64] L.A. Currie, G.A. Klouda, B.A. Benner Jr., K. Garrity, T.I. Eglinton, *Atmos. Environ.* 33 (1999) 2789.
- [65] A. Eiguren-Fernandez, A.H. Miguel, J.R. Froines, S. Thurairatnam, E.L. Avol, *Aerosol Sci. Technol.* 38 (2004) 447.
- [66] B. Glaser, A. Dreyer, M. Bock, S. Fiedler, M. Mehring, T. Heitmann, *Environ. Sci. Technol.* 39 (2005) 3911.
- [67] N. Marchand, J.L. Besombes, N. Chevron, P. Masclet, G. Aymoz, J.L. Jaffrezo, *Atmos. Chem. Phys.* 4 (2004) 1167.
- [68] B.M. Jenkins, A.D. Jones, S.Q. Turn, R.B. Williams, *Environ. Sci. Technol.* 30 (1996) 2462.
- [69] H.H. Yang, C.H. Tsai, M.R. Chao, Y.L. Su, S.M. Chien, *Atmos. Environ.* 40 (2006) 1266.
- [70] C. Schauer, R. Niessner, U. Pöschl, *Environ. Sci. Technol.* 37 (2003) 2861.
- [71] M. Goriaux, B. Jourdain, B. Temime, J.-L. Besombes, N. Marchand, A. Albinet, E. Leoz-Garziandia, H. Wortham, *Environ. Sci. Technol.* 40 (2006) 6398.
- [72] F. Reisen, J. Arey, *Environ. Sci. Technol.* 36 (2002) 4302.
- [73] B. De Foy, E. Caetano, V. Magana, A. Zitacuaro, B. Cardenas, A. Retama, R. Ramos, L.T. Molina, M.J. Molina, *Atmos. Chem. Phys.* 5 (2005) 2267.
- [74] T. Nielsen, *Atmos. Environ.* 22 (1988) 2249.
- [75] A. Greenberg, *Atmos. Environ.* 23 (1989) 2792.
- [76] A.L. Lafleur, J.B. Howard, J.A. Marr, T. Yadav, *J. Phys. Chem.* 97 (1993) 13539.
- [77] A.L. Lafleur, K. Taghizadeh, J.B. Howard, J.F. Anacleto, M.A. Quilliam, *J. Am. Soc. Mass Spectrom.* 7 (1996) 276.
- [78] J.L. Durant, A.L. Lafleur, E.F. Plummer, K. Taghizadeh, W.F. Busby Jr., W.G. Thilly, *Environ. Sci. Technol.* 32 (1998) 1894.
- [79] B.R.T. Simoneit, M. Kobayashi, M. Mochida, K. Kawamura, M. Lee, H.-J. Lim, B.J. Turpin, Y. Komazaki, *J. Geophys. Res. Atmos.* 109 (2004) D19S09.
- [80] C.L. Gigliotti, L.A. Totten, J.H. Offenberg, J. Dachs, J.R. Reinfelder, E.D. Nelson, T.R. Glenn IV, S.J. Eisenreich, *Environ. Sci. Technol.* 39 (2005) 5550.
- [81] J.M. Smedley, A. Williams, K.D. Bartle, *Combust. Flame* 91 (1992) 71.
- [82] A.L. Lafleur, J.B. Howard, K. Taghizadeh, E.F. Plummer, L.T. Scott, A. Necula, K.C. Swallow, *J. Phys. Chem.* 100 (1996) 17421.
- [83] B.R.T. Simoneit, P.M. Medeiros, B.M. Didyk, *Environ. Sci. Technol.* 39 (2005) 6961.
- [84] J.O. Allen, K.M. Dookeran, K.A. Smith, A.F. Sarofim, K. Taghizadeh, A.L. Lafleur, *Environ. Sci. Technol.* 30 (1996) 1023.

1 **Supplementary Information Section**

2 **Appendix 1. Subtraction Procedure of Non-PAH Organic Signal**

3 Here we explain the estimation procedure of the coefficients in the “fragmentation
4 tables” for PAHs used with the AMS data analysis software [50] and give an example of
5 how the coefficients are calculated. The “Fragmentation tables” used in this study are
6 given and described in Appendix 2. We calculate the background organic signal at the
7 m/z values of PAHs using a weighted average of the signals at adjacent non-PAH organic
8 peaks. The weighing accounts for the different distances between the surrounding organic
9 signals and the each PAH m/z . The weight for each surrounding organic signal was found
10 by taking the absolute value of the reciprocal difference in the peak distance. All the
11 coefficients were then normalized to sum to one.

12 Here we give an example for the mathematical formulation of the weighted
13 average used to find the non-PAH organic signal value at m/z 202. The non-PAH organic
14 signal at m/z 202 is estimated by weighting the organic signal at m/z values 194, 196, 204
15 and 206. We define the organic, PAH and total signal at a given m/z value as Org[m/z],
16 PAH[m/z] and Total[m/z], respectively. The background organic signals used to find the
17 non-PAH organic signal at m/z 202 are Org[194], Org[196], Org[204] and Org[206]. The
18 coefficients associated with each surrounding organic signal are C[194], C[196], C[204]
19 and C[206]. The mathematical formulae used to find the coefficients associated with each
20 surrounding organic signal for non-PAH organic signal at m/z 202 are:

$$21 \qquad C'[194] = \frac{1}{|202 - 194 - 1|} = 0.143 \qquad \text{(Eq. 1)}$$

$$22 \qquad C'[196] = \frac{1}{|202 - 196 + 1|} = 0.143 \qquad \text{(Eq. 2)}$$

$$C'[204] = \frac{1}{|202 - 204 - 1|} = 0.333 \quad (\text{Eq. 3})$$

$$C'[206] = \frac{1}{|202 - 206 + 1|} = 0.333 \quad (\text{Eq. 4})$$

The sum of C' coefficients is found and used to normalize each C' coefficient to sum to one:

$$C'[194] + C'[196] + C'[204] + C'[206] = 0.952 \quad (\text{Eq. 5})$$

$$C[194] = \frac{C'[194]}{0.952} = 0.15 \quad (\text{Eq. 6})$$

$$C[196] = \frac{C'[196]}{0.952} = 0.15 \quad (\text{Eq. 7})$$

$$C[204] = \frac{C'[204]}{0.952} = 0.35 \quad (\text{Eq. 8})$$

$$C[206] = \frac{C'[206]}{0.952} = 0.35 \quad (\text{Eq. 9})$$

32

33 Finally, the non-PAH organic signal at m/z 202 is defined as:

$$Org[202] = 0.15 * Org[194] + 0.15 * Org[196] + 0.35 * Org[204] + 0.35 * Org[206]$$

$$(\text{Eq. 10})$$

36

Appendix 2.

“Fragmentation tables” are used with the AMS data analysis software [50] to encode the subtraction procedure for the organics and PAHs at the m/z values relevant to AMS PAH analysis. The “fragmentation table” defines the AMS MS signals where Org is organic, and Total is the total signal at each m/z value (equal to the sum of the PAH and organic signals at that m/z value). The number in the square parenthesis following Org, PAH or Total refers to the m/z value of the AMS MS signal. In the Igor syntax for fragmentation tables, Org, PAH and Total used here are replaced with “frag_organic”, “frag_PAH” and “ m/z number value”, respectively, while the + signs used here are replaced by “,”.

m/z	Organic	PAH
198	0.35*Org[194]+0.35*Org[196]+0.15*Org[204]+0.15*Org[206]	Total[198]-Org[198]
199	0.35*Org[195]+0.35*Org[197]+0.15*Org[205]+0.15*Org[207]	Total[199]-Org[199]
200	0.25*Org[194]+0.25*Org[196]+0.25*Org[204]+0.25*Org[206]	Total[200]-Org[200]
201	0.25*Org[195]+0.25*Org[197]+0.25*Org[205]+0.25*Org[207]	Total[201]-Org[201]
202	0.15*Org[194]+0.15*Org[196]+0.35*Org[204]+0.35*Org[206]	Total[202]-Org[202]
203	Total[203]-PAH[203]	16*0.011*PAH[202]
212	0.35*Org[208]+0.35*Org[210]+0.15*Org[218]+0.15*Org[220]	Total[212]-Org[212]
213	0.35*Org[209]+0.35*Org[211]+0.15*Org[219]+0.15*Org[221]	Total[213]-Org[213]
214	0.25*Org[208]+0.25*Org[210]+0.25*Org[218]+0.25*Org[220]	Total[214]-Org[214]
215	0.25*Org[209]+0.25*Org[211]+0.25*Org[219]+0.25*Org[221]	Total[215]-Org[215]
216	0.15*Org[208]+0.15*Org[210]+0.35*Org[218]+0.35*Org[220]	Total[216]-Org[216]
217	Total[217]-PAH[217]	17*0.011*PAH[216]
222	0.37*Org[218]+0.37*Org[220]+0.13*Org[230]+0.13*Org[232]	Total[222]-Org[222]
223	0.37*Org[219]+0.37*Org[221]+0.13*Org[231]+0.13*Org[233]	Total[223]-Org[223]
224	0.29*Org[218]+0.29*Org[220]+0.21*Org[230]+0.21*Org[232]	Total[224]-Org[224]
225	0.29*Org[219]+0.29*Org[221]+0.21*Org[231]+0.21*Org[233]	Total[225]-Org[225]
226	0.21*Org[218]+0.21*Org[220]+0.29*Org[230]+0.29*Org[232]	Total[226]-Org[226]
227	0.21*Org[219]+0.21*Org[221]+0.29*Org[231]+0.29*Org[233]	Total[227]-Org[227]
228	0.13*Org[218]+0.13*Org[220]+0.37*Org[230]+0.37*Org[232]	Total[228]-Org[228]
229	Total[229]-PAH[229]	18*0.011*PAH[228]
236	0.36*Org[232]+0.36*Org[234]+0.14*Org[244]+0.14*Org[244]	Total[236]-Org[236]
237	0.36*Org[233]+0.36*Org[235]+0.14*Org[245]+0.14*Org[245]	Total[237]-Org[237]
238	0.27*Org[232]+0.27*Org[234]+0.23*Org[244]+0.23*Org[244]	Total[238]-Org[238]
239	0.27*Org[233]+0.27*Org[235]+0.23*Org[245]+0.23*Org[245]	Total[239]-Org[239]
240	0.18*Org[232]+0.18*Org[234]+0.32*Org[244]+0.32*Org[244]	Total[240]-Org[240]
241	0.18*Org[233]+0.18*Org[235]+0.32*Org[245]+0.32*Org[245]	Total[241]-Org[241]
242	0.09*Org[232]+0.09*Org[234]+0.41*Org[244]+0.41*Org[244]	Total[242]-Org[242]
243	Total[243]-PAH[243]	19*0.011*PAH[242]
246	0.41*Org[244]+0.41*Org[244]+0.09*Org[254]+0.09*Org[256]	Total[246]-Org[246]

247	0.41*Org[245]+0.41*Org[245]+0.09*Org[255]+0.09*Org[257]	Total[247]-Org[247]
248	0.32*Org[244]+0.32*Org[244]+0.18*Org[254]+0.18*Org[256]	Total[248]-Org[248]
249	0.32*Org[245]+0.32*Org[245]+0.18*Org[255]+0.18*Org[257]	Total[249]-Org[249]
250	0.23*Org[244]+0.23*Org[244]+0.27*Org[254]+0.27*Org[256]	Total[250]-Org[250]
251	0.23*Org[245]+0.23*Org[245]+0.27*Org[255]+0.27*Org[257]	Total[251]-Org[251]
252	0.14*Org[244]+0.14*Org[244]+0.36*Org[254]+0.36*Org[256]	Total[252]-Org[252]
253	Total[253]-PAH[253]	20*0.011*PAH[252]
260	0.37*Org[256]+0.37*Org[258]+0.13*Org[268]+0.13*Org[270]	Total[260]-Org[260]
261	0.37*Org[257]+0.37*Org[259]+0.13*Org[269]+0.13*Org[271]	Total[261]-Org[261]
262	0.29*Org[256]+0.29*Org[258]+0.21*Org[268]+0.21*Org[270]	Total[262]-Org[262]
263	0.29*Org[257]+0.29*Org[259]+0.21*Org[269]+0.21*Org[271]	Total[263]-Org[263]
264	0.21*Org[256]+0.21*Org[258]+0.29*Org[268]+0.29*Org[270]	Total[264]-Org[264]
265	0.21*Org[257]+0.21*Org[259]+0.29*Org[269]+0.29*Org[271]	Total[265]-Org[265]
266	0.13*Org[256]+0.13*Org[258]+0.37*Org[268]+0.37*Org[270]	Total[266]-Org[266]
267	Total[267]-PAH[267]	21*0.011*PAH[266]
272	0.38*Org[268]+0.38*Org[270]+0.12*Org[282]+0.12*Org[282]	Total[272]-Org[272]
273	0.38*Org[269]+0.38*Org[271]+0.12*Org[271]+0.12*Org[283]	Total[273]-Org[273]
274	0.31*Org[268]+0.31*Org[270]+0.19*Org[282]+0.19*Org[282]	Total[274]-Org[274]
275	0.31*Org[269]+0.31*Org[271]+0.19*Org[271]+0.19*Org[283]	Total[275]-Org[275]
276	0.23*Org[268]+0.23*Org[270]+0.27*Org[282]+0.27*Org[282]	Total[276]-Org[276]
277	0.23*Org[269]+0.23*Org[271]+0.27*Org[271]+0.27*Org[283]	Total[277]-Org[277]
278	0.15*Org[268]+0.15*Org[270]+0.35*Org[282]+0.35*Org[282]	Total[278]-Org[278]
279	Total[279]-PAH[279]	22*0.011*PAH[278]
284	0.41*Org[282]+0.41*Org[282]+0.09*Org[292]+0.09*Org[294]	Total[284]-Org[284]
285	0.41*Org[283]+0.41*Org[283]+0.09*Org[293]+0.09*Org[295]	Total[285]-Org[285]
286	0.32*Org[282]+0.32*Org[282]+0.18*Org[292]+0.18*Org[294]	Total[286]-Org[286]
287	0.32*Org[283]+0.32*Org[283]+0.18*Org[293]+0.18*Org[295]	Total[287]-Org[287]
288	0.23*Org[282]+0.23*Org[282]+0.27*Org[292]+0.27*Org[294]	Total[288]-Org[288]
289	0.23*Org[283]+0.23*Org[283]+0.27*Org[293]+0.27*Org[295]	Total[289]-Org[289]
290	0.14*Org[282]+0.14*Org[282]+0.36*Org[292]+0.36*Org[294]	Total[290]-Org[290]
291	Total[291]-PAH[291]	23*0.011*PAH[290]
296	0.37*Org[292]+0.37*Org[294]+0.13* Org[304]+0.13*Org[306]	Total[296]-Org[296]
297	0.37*Org[293]+0.37*Org[295]+0.13* Org[305]+0.13*Org[307]	Total[297]-Org[297]
298	0.29*Org[292]+0.29*Org[294]+0.21* Org[304]+0.21*Org[306]	Total[298]-Org[298]
299	0.29*Org[293]+0.29*Org[295]+0.21* Org[305]+0.21*Org[307]	Total[299]-Org[299]
300	0.21*Org[292]+0.21*Org[294]+0.29* Org[304]+0.29*Org[306]	Total[300]-Org[300]
301	0.21*Org[293]+0.21*Org[295]+0.29* Org[305]+0.29*Org[307]	Total[301]-Org[301]
302	0.13*Org[292]+0.13*Org[294]+0.37* Org[304]+0.37*Org[306]	Total[302]-Org[302]
303	Total[303]-PAH[303]	24*0.011*PAH[302]
312	0.35*Org[308]+0.35*Org[310]+0.15* Org[318]+0.15*Org[320]	Total[312]-Org[312]
313	0.35*Org[309]+0.35*Org[311]+0.15* Org[319]+0.15*Org[321]	Total[313]-Org[313]
314	0.25*Org[308]+0.25*Org[310]+0.25* Org[318]+0.25*Org[320]	Total[314]-Org[314]
315	0.25*Org[309]+0.25*Org[311]+0.25* Org[319]+0.25*Org[321]	Total[315]-Org[315]
316	0.15*Org[308]+0.15*Org[310]+0.35* Org[318]+0.35*Org[320]	Total[316]-Org[316]
317	Total[317]-PAH[317]	25*0.011*PAH[316]
322	0.36*Org[318]+0.36*Org[320]+0.14* Org[330]+0.14*Org[330]	Total[322]-Org[322]
323	0.17*Org[319]+0.17*Org[319]+0.33* Org[321]+0.33*Org[321]	Total[323]-Org[323]
324	0.27*Org[318]+0.27*Org[320]+0.23* Org[330]+0.23*Org[330]	Total[324]-Org[324]
325	0.20*Org[319]+0.20*Org[319]+0.30* Org[321]+0.30*Org[321]	Total[325]-Org[325]
326	0.18*Org[318]+0.18*Org[320]+0.32* Org[330]+0.32*Org[330]	Total[326]-Org[326]
327	0.21*Org[319]+0.21*Org[319]+0.29* Org[321]+0.29*Org[321]	Total[327]-Org[327]
328	0.09*Org[318]+0.09*Org[320]+0.41* Org[330]+0.41*Org[330]	Total[328]-Org[328]
329	Total[329]-PAH[329]	26*0.011*PAH[328]

Several groups of PAH peaks do not have four different non-PAH organic signal used to define the organic signal at the m/z values of PAHs due to the lack of available non-PAH organic signals. Those groups of peaks are the following (reason for including less groups of peaks is in the parenthesis):

- 240+242 (only one even and one odd non-PAH organic signal available at m/z values 244 and 245)

- 250+252 (only one even and one odd non-PAH organic signal available at m/z values 244 and 245)

- 276+278 (strong aerosol signal in some cases coming from phthalates at m/z values 280 and 281 makes them unsuitable for our purposes as they do not fit the pattern of a slowly decaying non-PAH organic signal; thus, only one even and one odd non-PAH organic signal are available at m/z values 282 and 283)

- 288+290 (strong aerosol signal coming from phthalates at m/z values 280 and 281 makes them unavailable to use; thus, only one even and one odd non-PAH organic signal are available at m/z values 282 and 283)

- 326+328 (signal was not recorded beyond m/z 330; thus, only one even non-PAH organic signal is available at m/z value 330, and total of only two odd non-PAH organic signals are available at m/z values 319 and 321)

This fragmentation table for organics and PAHs can be downloaded from:

<http://cires.colorado.edu/jimenez-group/SI/>

(Please note that there are two sets of fragmentation tables available depending on the maximum m/z scanned: one that goes up to m/z 301 and one that goes up to m/z 331.)

Appendix 3.

We have developed a rigorous estimate of the uncertainty due to the subtraction procedure, based on the propagation of uncertainty from the estimated noise in each m/z (from Allan et al. [54]). We used the uncertainty propagation to calculate the uncertainties associated with each group of APAH peaks, and with the total and modified total PAH (APAH and APAH*, respectively).

The uncertainty propagation follows from the mass concentration of the single m/z value APAH peak defined as:

$$PAH[m/z] = Total[m/z] - Org[m/z] \quad (Eq. 11)$$

$$Org[m/z] = C_1 * Org[m/z]_1 + C_2 * Org[m/z]_2 + C_3 * Org[m/z]_3 + C_4 * Org[m/z]_4$$

(Eq. 12)

where $Org[m/z]$, $PAH[m/z]$ and $Total[m/z]$ are organic, PAH and total signal at a given m/z value, respectively. C_1 , C_2 , C_3 and C_4 are the weighting coefficients used to get the non-PAH organic average at certain PAH m/z value, as described in Appendix 1.

To obtain the mass concentration for the group of APAH peaks with the same molecular weight, the signal from all m/z values needs to be added together:

$$PAH_{GROUP} = \sum_{m/z} PAH[m/z] \quad (Eq. 13)$$

Finally, to obtain the total and modified total PAH mass concentrations of all the PAH groups of peaks and modified groups of peaks, respectively, are added together:

$$PAH_A = \sum_{ALL\,GROUPS} PAH_{GROUP} \quad (Eq. 14)$$

$$PAH_A^* = \sum_{MODIFIED\,GROUPS} PAH_{MODIFIED\,GROUPS} \quad (Eq. 15)$$

where ALL GROUPS refers to the groups of APAH with MW 202, 216, 226+228, 240+242, 250+252, 264+266, 276+278, 288+290, 300+302, 316 and 326+328, and MODIFIED GROUPS refers to the groups with MW 202, 226+228, 250+252, 276+278 and 300+302.

From the above definitions the uncertainty of single PAH peak, $\sigma_{\text{PAH}[m/z]}^2$, will be:

$$\sigma_{\text{PAH}[m/z]}^2 = \sigma_{\text{Total}[m/z]}^2 + \sigma_{\text{Org}[m/z]}^2 = \sigma_{\text{Total}[m/z]}^2 + C_1^2 \sigma_{\text{Org}[m/z]_1}^2 + C_2^2 \sigma_{\text{Org}[m/z]_2}^2 + C_3^2 \sigma_{\text{Org}[m/z]_3}^2 + C_4^2 \sigma_{\text{Org}[m/z]_4}^2 \quad (\text{Eq. 16})$$

The uncertainty of the group of PAH peaks with the same MW, $\sigma_{\text{PAH}_{\text{GROUP}}}^2$, will be:

$$\sigma_{\text{PAH}_{\text{GROUP}}}^2 = \sum_{m/z} \sigma_{\text{PAH}[m/z]}^2 \quad (\text{Eq. 17})$$

Finally, the uncertainty of the total and modified total PAH, $\sigma_{\text{PAH}_A}^2$ and $\sigma_{\text{PAH}_A^*}^2$, respectively, will be:

$$\sigma_{\text{PAH}_A}^2 = \sum_{\text{ALL GROUPS}} \sigma_{\text{PAH}_{\text{GROUP}}}^2 \quad (\text{Eq. 18})$$

$$\sigma_{\text{PAH}_A^*}^2 = \sum_{\text{MODIFIED GROUPS}} \sigma_{\text{PAH}_{\text{MODIFIED GROUP}}}^2 \quad (\text{Eq. 19})$$

The PAH signals that are estimated as the ^{13}C isotopic contribution from the PAH signal at their molecular ions (at m/z values 203, 217, 229, 243, 253, 267, 279, 291, 303, 317 and 329) are calculated as:

$$\text{PAH}[m/z, ^{13}\text{C}] = n * 0.011 * \text{PAH}[(m/z, ^{13}\text{C}) - 1] \quad (\text{Eq. 20})$$

where n is the number of C atoms in a PAH. The uncertainty of the PAH signal at the ^{13}C isotopic contribution m/z values (given above), $\sigma_{\text{PAH}[m/z, ^{13}\text{C}]}^2$, is calculated as:

$$\sigma_{\text{PAH}[m/z, ^{13}\text{C}]}^2 = n^2 * 0.011^2 * \sigma_{\text{PAH}[(m/z, ^{13}\text{C}) - 1]}^2 \quad (\text{Eq. 21})$$

Supplementary Information Figure captions

Figure SI-1: Left: laboratory Q-AMS and NIST MS of triphenylene and 10-methylbenz[*a*]anthracene (abbreviated as 10-Mb[*a*]a in the scatter plot) standards. Right: scatter plots between the AMS and NIST database mass spectra of PAH standards.

Figure SI-2: Left: laboratory Q-AMS and NIST MS of benzo[*e*]pyrene, benzo[*ghi*]perylene and coronene standards. Right: scatter plots between the AMS and NIST database mass spectra of PAH standards.

Figure SI-3: The fraction of negative concentrations for the total and modified total APAH (APAH and APAH*, respectively), and for all the groups of PAHs with the same MW vs. their average total concentration. The molecular weights of PAHs clustered around the 40% fraction of negative PAHs are (from the ones with lowest to the highest fraction of negative PAHs): 264+266, 326+328, 316 and 288+290. All the data shown in Figure SI-3 can be found in Table 2. The analysis is done for the 4-points smoothed 4-min data presented in this paper.

Figure SI-4: Comparison of the molecular ion mass spectral regions for the NIST EI MS [39] and different Q-AMS PAH mass spectra. The abundance of the main peak in the spectra was set to 100% and other peaks were scaled accordingly. NIST EI and Q-AMS EI mass spectra for the PAHs with MWs of 202, 226, 252 and 276, for which the base peak is the molecular ion in all cases, are compared in Figures SI-4a, 4b, 4c, and 4d,

134 respectively. Shown are the ambient Q-AMS MS of the highest MCMA-2003 Q-AMS-
135 measured PAH mass concentrations during the early morning of April 13, 2003 (Figure
136 3a), and the average MS of all 5 AM – 9 AM periods during MCMA-2003 (Figure 3b).
137 Also shown are laboratory Q-AMS MS of selected groups of peaks for PAHs generated
138 in laboratory propane flame study [19], c-ToF-AMS [28] at Aerodyne pyrene spectra [M.
139 Northway, Aerodyne Research, personal communication, 2004], HR-ToF-AMS at CU-
140 Boulder [29] pyrene spectra, and a Q-AMS at CU-Boulder pyrene, benzo[*e*]pyrene and
141 benzo[*ghi*]perylene spectra. Note that the laboratory Q-AMS and NIST database spectra,
142 as opposed to the ambient Q-AMS spectra, do not have the subtraction procedure applied.
143

144 Figure SI-5: Figures SI-5a, 5b, 5c and 5d compare the molecular ion mass spectral
145 regions for the NIST EI MS [39] and different Q-AMS PAH mass spectra for the PAHs
146 with MWs of 216, 228, 242 and 300, respectively. The base peak was set to 100% and
147 other peaks were scaled accordingly. Shown in Figures SI-5a and SI-5d are the ambient
148 Q-AMS MS of the highest MCMA-2003 Q-AMS-measured PAH mass concentrations
149 during the early morning of April 13, 2003, and the average MS of all 5 AM – 9 AM
150 periods during MCMA-2003. Also shown in Figures SI-5a and SI-5d are laboratory Q-
151 AMS MS of selected groups of peaks for PAHs generated in laboratory propane flame
152 study [19] and a Q-AMS at CU-Boulder 1-methylpyrene, 2,3-benzofluorene and
153 coronene spectra. Figures SI-5b and SI-5c compare only NIST and Q-AMS laboratory
154 MS of pure PAH standards triphenylene (MW=228) and 10-methylbenz[*a*]anthracene
155 (MW=242), respectively. Both of these PAHs are defined within the group of PAHs with
156 2 molecular weights in the ambient data (PAHs with MW 226+228 and 240+242,

respectively), and the PAHs with the lower MW will give the strongest peak in the ambient MS (PAHs with MW 226 and 240, respectively). In Figures SI-5b and 5c ambient and flame laboratory Q-AMS MS are not shown, because the presence of strong peaks originating from PAHs with MWs 226 and 240 makes the figures hard to read due to reasons unrelated to the real degree of agreement. Note that the laboratory Q-AMS and NIST database spectra do not have the subtraction procedure applied.

Figure SI-6: Degree of PAH fragmentation for Q-AMS and NIST laboratory PAH spectra vs molecular weight. Also shown is the constant fragmentation factor of 1.77 used in Marr et al. [18].

Figure SI-7: Measured Q-AMS PAH relative ionization efficiencies (RIEs) vs PAH molecular weight (MW). Error bars were calculated as the uncertainties in the ionization efficiency relative to nitrate, in the number of particles counted, and in the particle mass and number concentration corrections.

Figure SI-8: Comparisons of selected individual FPAH and APAH. The scatter plots show correlations between FPAH and APAH with molecular weights of 216, 240+242 and 300+302 (note that for the comparison of PAHs with main MW 300, we are comparing FPAHs with MW 300 to APAHs with MW 300+302). For the FPAH with molecular weight 216, two types of samples are shown: FPAH samples collected on filter (cross) and the sum of FPAH samples collected on filter + PUF (circle), both with 8 data points. There are only 4 APAH points that overlap with filter and PUF samples. For the

comparison of PAHs with MW 216 filter and PUF samples are represented in two ways: full circles show the sum of filter + PUF mass concentration as collected in the field, and open circles show the results of applying partitioning theory [51] and the average MCMA-2003 conditions for FPAH filter collection periods to the sum of filter + PUF mass concentrations. The line equations for the comparisons of PAHs with MW 216 are given here: Filter FPAH data (crosses): $FPAH_{216} = (0.05 \pm 0.02) * APAH_{216}$; Partitioned filter + PUF data (open circles): $FPAH_{216} = (0.16 \pm 0.09) * APAH_{216}$. All the regression lines have the intercept forced through zero.

Figure SI-9: Average Q-AMS mass spectra for the periods when Q-AMS sampling overlapped with FPAH filter sampling periods (April 27 and April 29, 2003). Same time periods FPAH and APAH mass concentrations are shown in Figures 9 and SI-8.

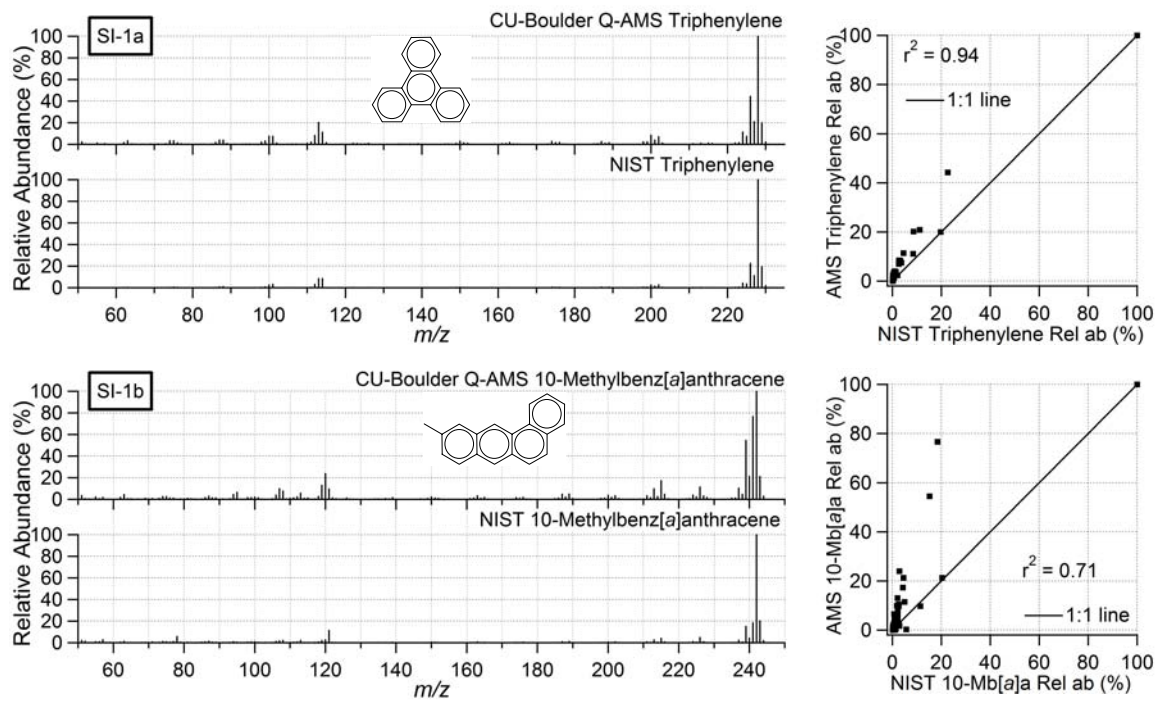


Figure SI-1

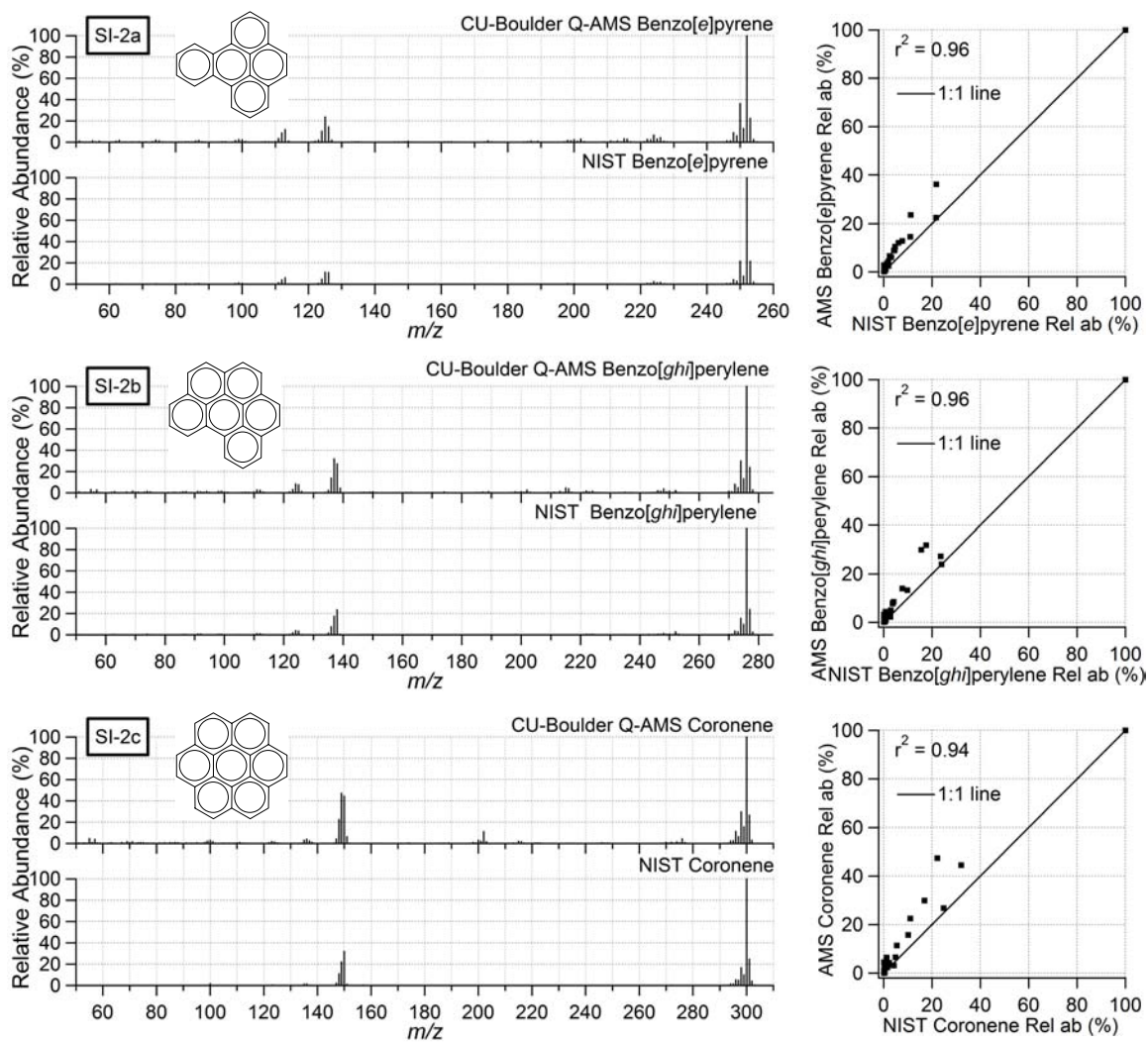


Figure SI-2

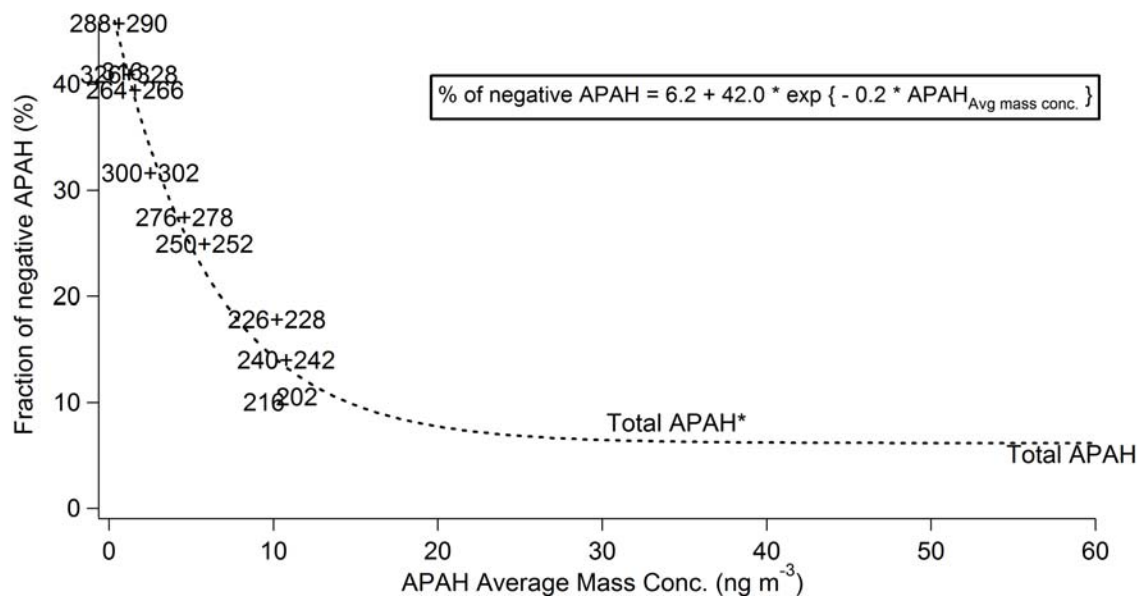


Figure SI-3

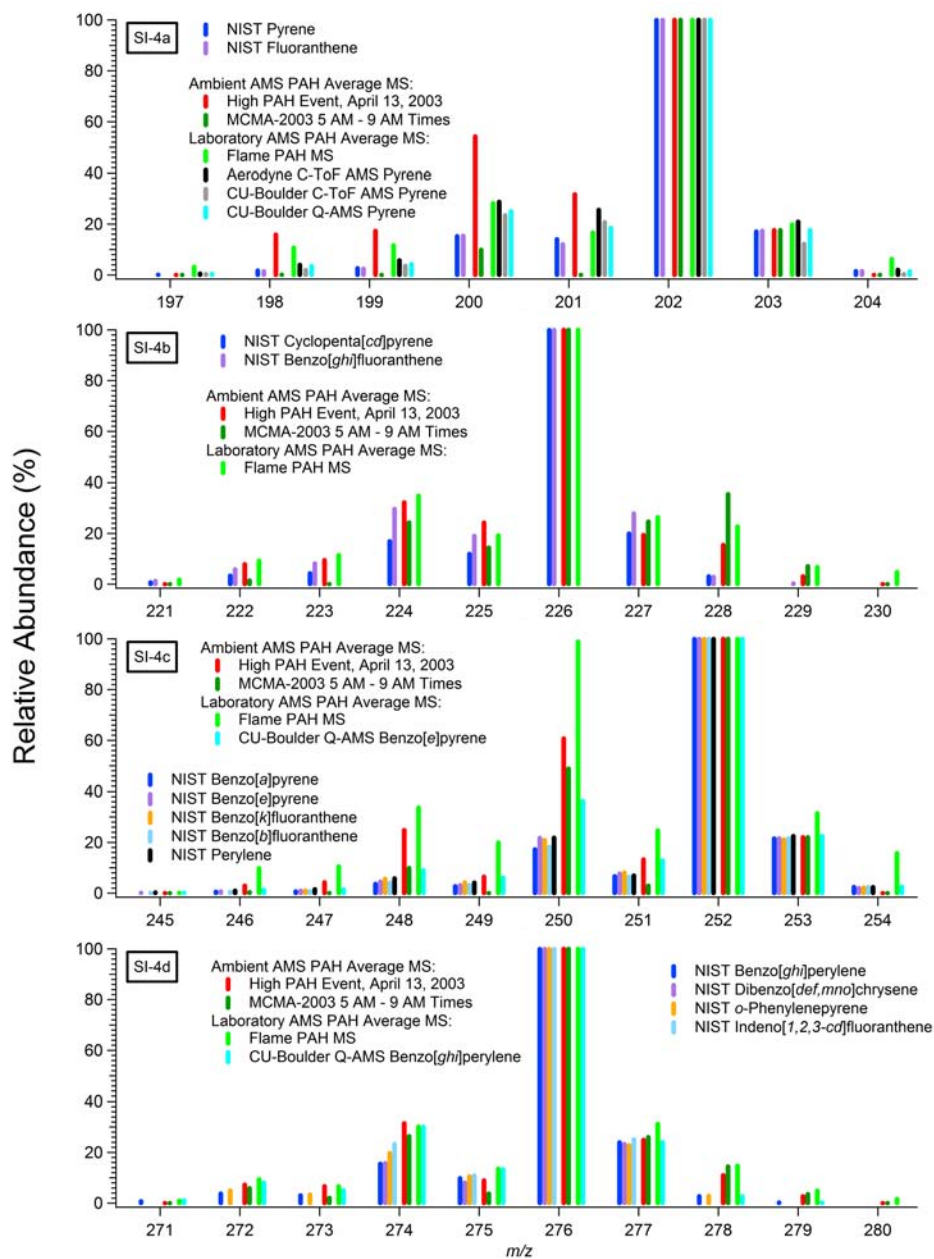


Figure SI-4

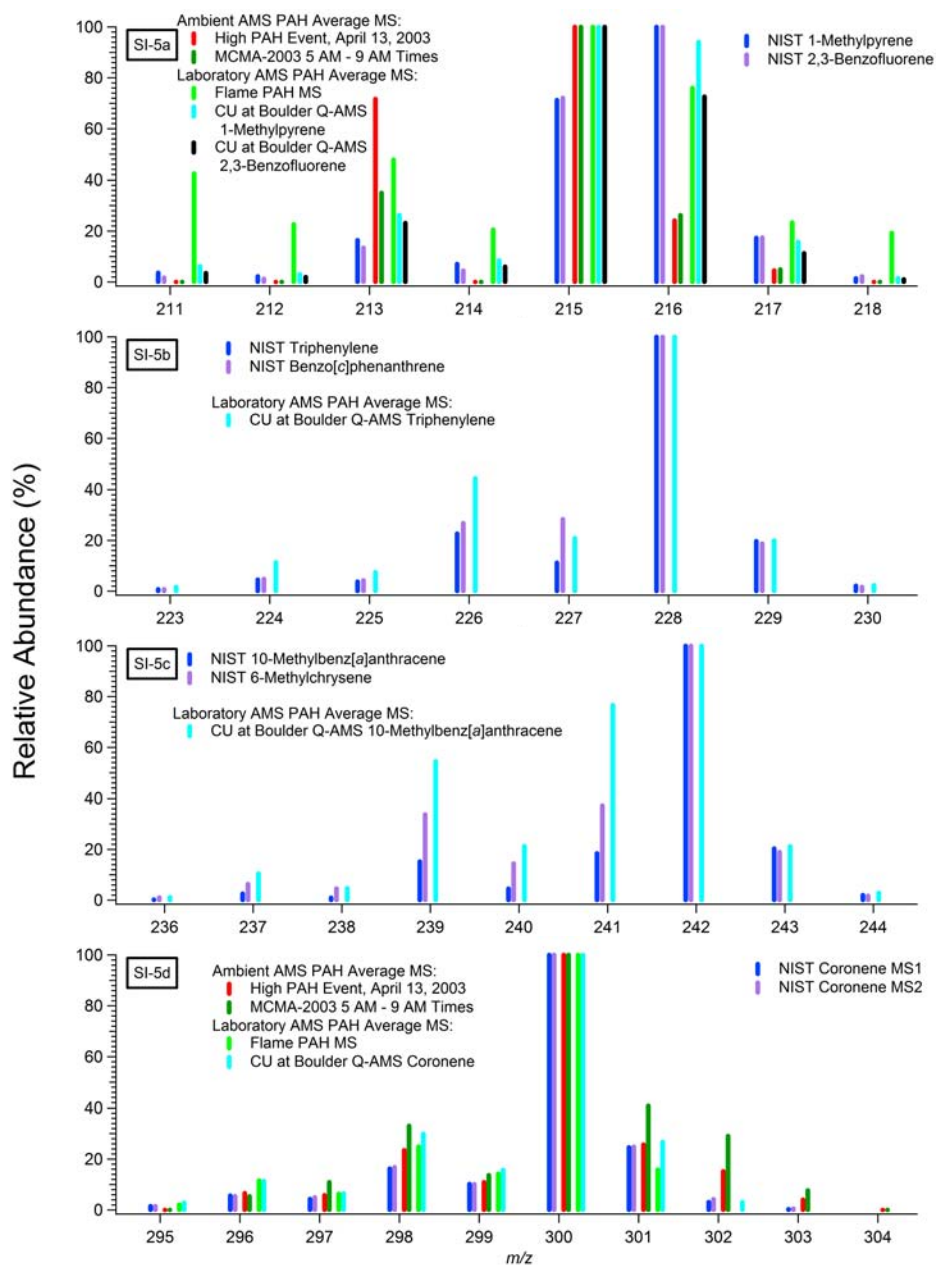


Figure SI-5

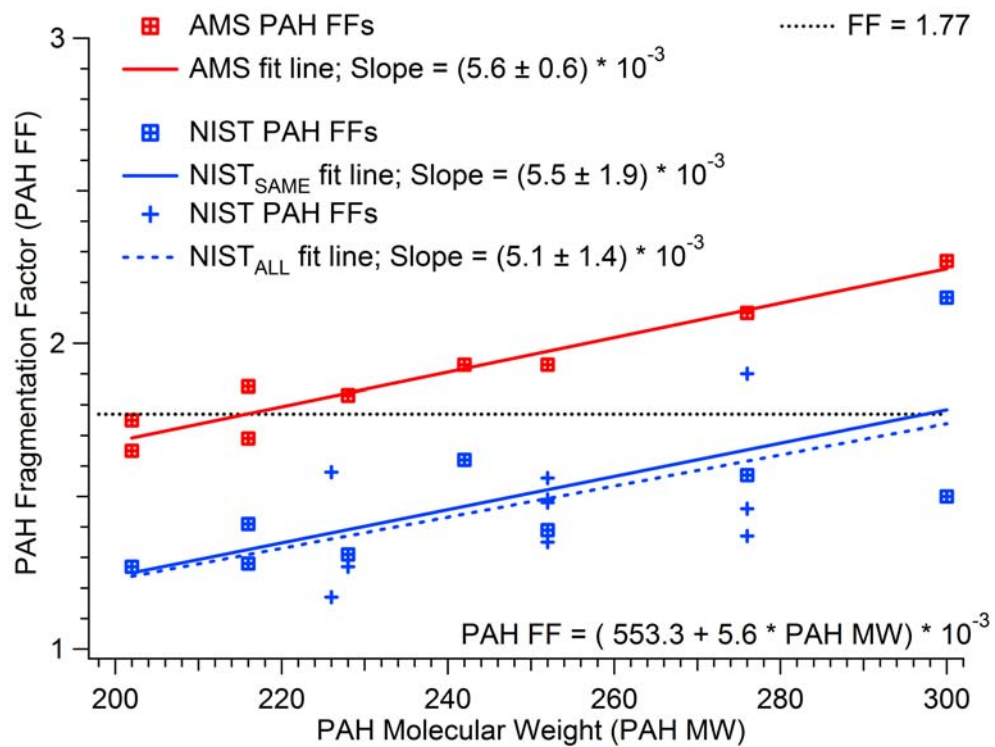


Figure SI-6

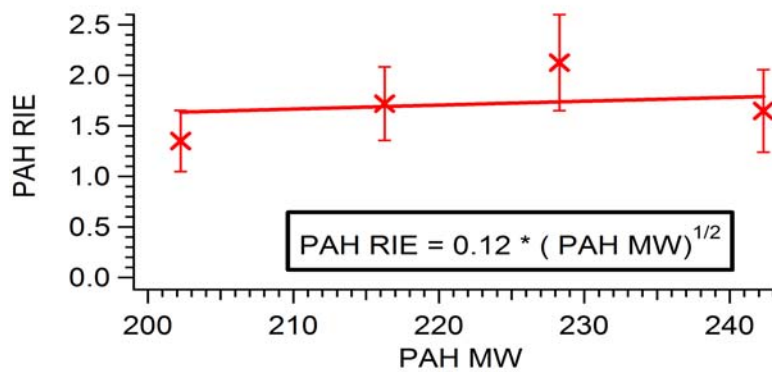


Figure SI-7

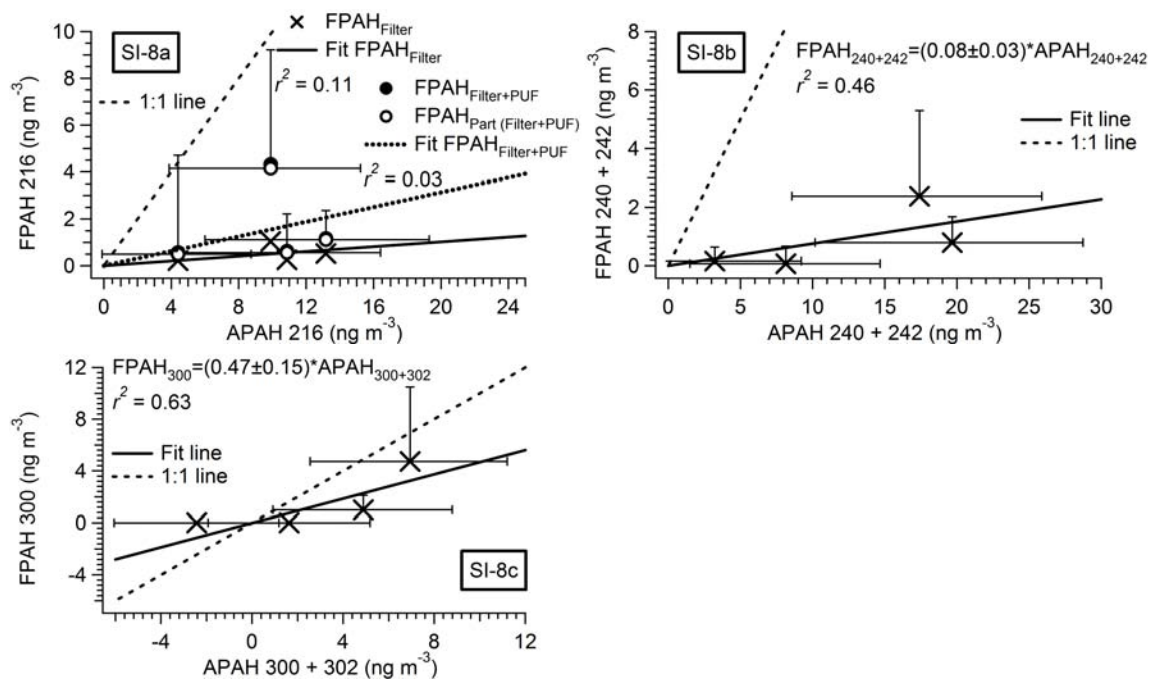


Figure SI-8

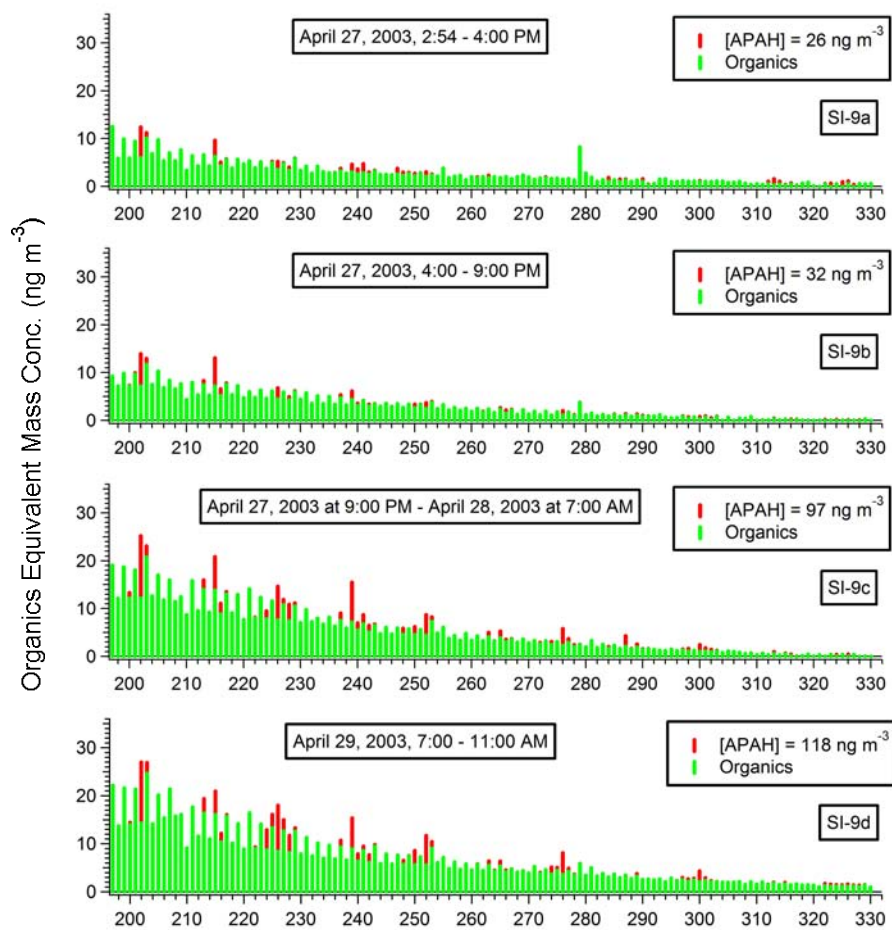


Figure SI-9